Correction published 14 May 2004

Tectonic control on past circulation of the Mediterranean Sea: A model study of the Late Miocene

P. Th. Meijer

Vening Meinesz Research School of Geodynamics, Faculty of Geosciences, Utrecht University, Utrecht, Netherlands

R. Slingerland

Department of Geosciences, Pennsylvania State University, University Park, Pennsylvania, USA

M. J. R. Wortel

Vening Meinesz Research School of Geodynamics, Faculty of Geosciences, Utrecht University, Utrecht, Netherlands

[1] We examine the effect of Late Miocene paleogeography on the circulation and water properties of the Mediterranean Sea by using an ocean circulation model. Results obtained for the past are compared to a control experiment with the present-day geometry. To focus on paleogeography, atmospheric forcing is always based on the present-day climatology. We seek insight that allows us to test ideas based on observations and to formulate new working hypotheses. The Late Miocene is examined first, since it represents an important stage in the evolution of the Mediterranean. The present-day model reproduces the main aspects of the surface to intermediate depth circulation and water properties. The model does not capture the deep circulation known to occur at present in both subbasins. When the subbasins are reconstructed to their Late Miocene shape (keeping intervening sills at present-day levels) the overall nature of the surface/intermediate depth circulation proves unaffected. The model, however, predicts intense deep circulation in the eastern Mediterranean, most likely due to the greater surface area of the reconstructed Adriatic Sea. Using the first paleoexperiment as a starting point several additional paleogeographical aspects are examined.   *INDEX TERMS:* 4243 Oceanography: General: Marginal and semienclosed seas; 4267 Oceanography: General: Paleoceanography; 4255 Oceanography: General: Numerical modeling; 8150 Tectonophysics: Plate boundary—general (3040); *KEYWORDS:* paleoceanography, circulation modeling, Mediterranean Sea

Citation: Meijer, P. Th., R. Slingerland, and M. J. R. Wortel (2004), Tectonic control on past circulation of the Mediterranean Sea: A model study of the Late Miocene, *Paleoceanography*, *19*, PA1026, doi:10.1029/2003PA000956.

1. Introduction

[2] Throughout Cenozoic time, slow convergence between the African plate and the Eurasian plate has gradually shaped the intervening stretch of Tethys Ocean into the present Mediterranean Sea. Ensuing processes such as orogeny, back-arc spreading, and island arc migration have resulted in a series of fairly small subbasins connected by narrow and often shallow straits. These tectonically induced changes in basin geometry, together with changes in climate, have left their signature in the sedimentary record. For example, a variety of paleoceanographic proxy records hold evidence for changes in the exchange of water with the Atlantic ocean [e.g., *Kouwenhoven et al.*, 1999, 2003; *Seidenkrantz et al.*, 2000; *Sierro et al.*, 2003]. In particular from the Late Miocene onwards, the Mediterranean basin witnessed the regular deposition of organic-rich sapropels. Sapropels are commonly considered to be controlled by climate variation, correlating as they do with Earth's precession cycle [*Rossignol-Strick*, 1983; *Hilgen*, 1991]. However, the very fact that sedimentation in the Mediterranean

displays such sensitivity to insolation changes is thought to be due to the basin's (paleo-)geography. The start of the regular occurrence of sapropels during the Late Miocene seems to indicate that the isolation of the Mediterranean as a whole and that of its subbasins reached a critical level (J. E. Meulenkamp, personal communication, 1999). An extreme paleoceanographic signal is constituted by the presence of the Messinian evaporites. Although much debated the deposition of these evaporites is most likely significantly controlled by tectonic activity in the area of southern Iberia-northwest Africa [e.g., *Krijgsman et al.*, 1999; *Duggen et al.*, 2003].

[3] Here we try to link these effects with their causes by using an ocean general circulation model to assess the effects of temporal changes in basin geometry on the circulation and distribution of water properties of the Mediterranean Sea. In a subsequent study we will address the role of changes in climate. Along this way we hope to establish a background against which we can evaluate available and new paleoceanographic observations. The model allows us to formulate expectations as to the role of specific elements of the past configuration and to test ideas developed on the basis of the geological observations. At the present stage the question we will pose is a general

one: What changes in circulation may we expect to result from the evolving tectonics, independent of the evolving climate?

[4] In this first investigation we concentrate on the Late Miocene, more specifically, on the Tortonian (about 8 Ma). There are various reasons for this. The Tortonian was a period when the geometry was significantly different from present: back-arc opening of the Tyrrhenian Sea and Aegean Sea had only just started (Figure 1, top, identifies the main geographical elements). Consequently, the Adriatic Sea was much wider than at present. Instead of the present connection at Gibraltar there were two seaways connecting the Mediterranean to the Atlantic Ocean: the Betic gateway and the Moroccan gateway. However, during the Late Miocene, the configuration was similar to the actual situation in one important way: the basin had already lost its connection to the Indian Ocean. Finally, the Tortonian situation allows us to investigate the stage immediately preceding the Messinian salinity crisis.

[5] In this investigation, in order to isolate the effect of paleogeography on Mediterranean circulation, we will combine both the present-day geometry and a reconstruction of the Late Miocene geometry with the present-day climatological state of the atmosphere. Moreover, to be able to study this important factor separately in more detail, we will start out assuming all straits in the paleoexperiments to have the depth of the present-day straits of Gibraltar and Sicily: about 300 m. Our study is the first to apply a circulation model to the Mediterranean basin millions of years back in time, and as such, the experiments described here are meant to lay the basis for subsequent investigations of the role of climate and strait depth. Although numerous paleocirculation modeling studies exist for epeiric seas and the deep oceans (recently, e.g., *Slingerland et al.* [1996]; *Bice et al.* [2000]; *Bjerrum et al.* [2001]; *Poulsen et al.* [2001]) none has addressed these questions for an ocean basin of Mediterranean type.

[6] We will construct our numerical model by building upon the extensive research dedicated to modeling the circulation of the present-day Mediterranean Sea [e.g., *Roussenov et al.*, 1995; *Zavatarelli and Mellor*, 1995; *Haines and Wu*, 1995; *Pinardi and Masetti*, 2000; *Beckers et al.*, 2002, and references therein]. Existing models for the past state of the Mediterranean all focus on the role of changes in climate [e.g., *Bigg*, 1994; *Myers et al.*, 1998; *Stratford et al.*, 2000; *Myers*, 2002]. They do not go further back in time than the last glacial maximum (20,000 years ago). These models essentially use the present-day geometry although sea level lowering is accounted for when appropriate.

2. Model Description

2.1. Ocean Circulation Model

[7] For our study we use the Mediterranean version of MOMA. MOMA has been developed by David Webb [e.g., *Webb*, 1996] and is in turn a version of the Modular Ocean Model (MOM) [*Pacanowski and Griffies*, 1998] optimized for "A"rray processor computers (an aspect not exploited in our work), and featuring a free surface. The Mediterranean version of MOMA was developed at The University of
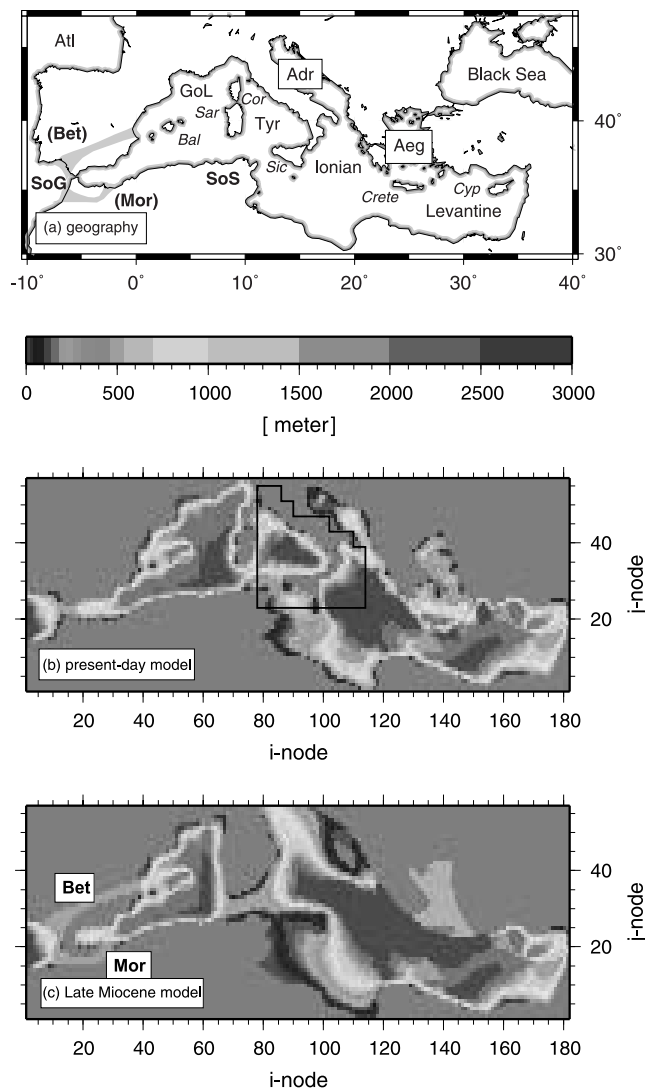

Figure 1. (top) Geographical names used in the text. The approximate position of the Late Miocene Atlantic gateways is also shown (shaded). Key: Adr, Adriatic Sea; Aeg, Aegean Sea; Atl, Atlantic Ocean; Bal, Balearic islands; Bet, Betic gateway, Cor, Corsica; Cyp, Cyprus; GoL, Gulf of Lions; Mor, Moroccan gateway; Sar, Sardinia; Sic, Sicily; SoG, Strait of Gibraltar; SoS, Strait of Sicily; Tyr, Tyrrhenian Sea. (middle) Model bathymetry for the present day. The black contour delimits the area for which atmospheric data are masked. (bottom) Model bathymetry for the Late Miocene (reference paleogeography). Key: Bet, Betic gateway, Mor, Moroccan gateway. See color version of this figure at back of this issue.

Edinburgh (for an overview, see *Haines and Wu* [1998]) and is made available to the community by Kevin Stratford as part of the Mediterranean Modeling Network ("MedNet"; http://www.met.ed.ac.uk/mednet). MOMA treats the fundamental equations in largely unsimplified form. The main prognostic variables are the horizontal velocity vectors u and v, the potential temperature T, and the salinity S, all as functions of space and time. These are obtained from the

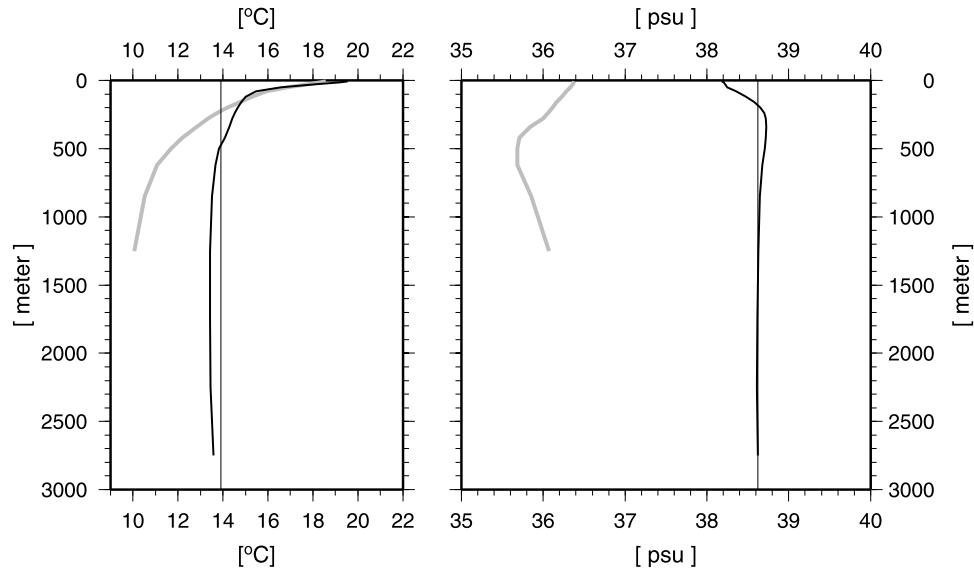**Figure 2.** Bold line: horizontally averaged temperature and salinity of the Mediterranean basin used as initial conditions. Thin line: values obtained by averaging throughout the basin volume (13.91°C and 38.62 psu). Shaded line: annual mean conditions in the Atlantic box used for restoration (not used below 1250 m).

momentum equation and the conservation equations for seawater, heat, and salt. The momentum equation is subject to two common approximations: (1) density is considered a constant except in the evaluation of buoyancy forces (Boussinesq approximation), and (2) the vertical component of the momentum equation is taken to reduce to the statement that pressure at a certain point is equal to the weight of the overlying water column (hydrostatic approximation).

[8] In our implementation of MOMA we use a biharmonic formulation to parameterize the horizontal turbulent diffusion of momentum and of heat and salt. In the vertical a Laplacian diffusion is used. Diffusivities are uniform and constant. Values used are those of *Roussenov et al.* [1995]; momentum, horizontal: 8×10^{18} cm^4 s^{-1}; heat/salt, horizontal: 2.4×10^{19} cm^4 s^{-1}; momentum, vertical: 1.5 cm^2 s^{-1}; heat/salt, vertical: 1 cm^2 s^{-1}. Whenever the vertical density structure is found unstable, the water column is homogenized in terms of temperature and salinity. In order to keep the model straightforward and as close as possible to the original implementation of *Roussenov et al.* [1995], two options of the Mediterranean MOMA code have not been used. These are the parameterization of eddies and the use of a flux-limited advection scheme.

2.2. Model Geometry Present-Day Experiments

[9] Our present-day geometry (Figure 1, middle) is the one devised by *Roussenov et al.* [1995] and is provided with the Mediterranean-MOMA code. The horizontal resolution is $^1/_4° \times ^1/_4°$, which results in 182 (east-west) by 57 (north-south) grid points. There are 19 horizontal levels. Spacing between the deepest levels is 500 m; the spacing decreases to 10 m for the shallowest levels so as to be able to resolve the mixed layer and thermocline. The deepest level is at 3000 m meaning that some deeper features of the sea are not

represented. The shallow northern part of the Adriatic Sea is not taken into account either. The model has a closed western boundary. Within the Atlantic "box" thus formed, temperature and salinity are restored to present-day annual mean climatological values (Figure 2) for all runs, including the paleoexperiments. The restoration timescale is 1 day at the westernmost 9 grid columns and then decreases to zero at column 14.

2.2.1. Late Miocene Experiments

[10] For the Late Miocene experiments we developed an approximation of the Tortonian paleogeography (Figure 1, bottom). The present-day model was taken as a starting point and modified in three key areas: the connection to the Atlantic Ocean, the central Mediterranean, and the area of the Aegean Sea. The past geometry was gleaned from the Late Tortonian sheet of the Peri-Tethys Atlas [*Dercourt et al.*, 2000]. As explained in the introduction, all major straits were first set at 300 m depth. For the central Mediterranean portion, depths were assigned to some of the contours used by *Dercourt et al.* [2000]. The limit of "shallow marine carbonate deposits" was taken to correspond to 100 m; the change from "deep marine" to "deep oceanic basin" to 2500 m. On the basis of paleobathymetric estimates by *van der Meulen et al.* [1999] the Apenninic foredeep was placed at 1000 m. We then fitted an adjustable tension surface through the available points [*Smith and Wessel*, 1990]. As in the present-day model, the Adriatic Sea has been clipped-off to the north. The Aegean Sea is included with the geometry given by *Dercourt et al.* [2000] and a uniform depth of 500 m. The basin geometry thus obtained will be referred to as our "reference paleogeography," the corresponding experiment the "reference paleorun."

[11] In the course of the Late Miocene both the Tyrrhenian Sea and the Aegean Sea opened through back-arc extension. In our model experiments we will always con-

sider the Tyrrhenian Sea to be fully closed. The situation of a still closed Aegean Sea is the subject of a separate experiment. In this additional run we exclude an inflow from the Paratethys region (early Black Sea and adjacent area). A second additional experiment considers the possibility of shallow straits crossing the Corsica-Sardinia block, inferred in particular on the basis of the distribution of mammal fossils [Rögl, 1999]. Finally, in a third additional experiment we examine the effect of lowering the strait that connects the western and eastern subbasin. The past depth of this connection is uncertain; it may well have been deeper than the present-day value of 300 m (W. Krijgsman, personal communication, 2002). The resulting paleomodels are rough but capture the main changes in geometry compared to the present day (except, perhaps, in terms of the depth of the Atlantic gateways).

2.2.2. Initial Conditions

[12] Whereas we could start our present-day control experiment from the observed three-dimensional temperature and salinity distribution, we have no such a priori information at our disposal for the Late Miocene. Therefore we choose to initialize both the present-day runs and the paleoruns from fields that are obtained by averaging the annual mean climatological fields on horizontal levels. Data are obtained from the Mediterranean Oceanic Data Base, release MED5 [Brasseur et al., 1996] (see http://modb.oce.ulg.ac.be) as provided with the Mediterranean version of MOMA. The resulting variations with depth are shown in Figure 2. Profiles similar to these horizontal averages are found in the full three-dimensional distribution in the area of the central Ionian Sea.

[13] The choice of initial conditions was found to prove relevant. As an alternative to horizontally averaged initial conditions we have considered the case of homogeneous temperature and salinity (basin averages of the annual mean climatology; also indicated in Figure 2). In this case, however, we did not obtain a stable or realistic present-day control experiment.

2.3. Atmospheric Forcing

[14] We wish to combine each of the two model geometries, i.e., the present-day geometry and our approximation of the Late Miocene geometry, with the present-day atmospheric forcing. This implies that the fluxes by which the atmosphere drives the ocean circulation: net heat flux, freshwater flux, and wind stress (flux of momentum), must be calculated interactively during the experiment. Because precipitation is known poorly, most published models use a relaxation to the observed sea surface salinity (SSS) rather than a freshwater flux [e.g., Roussenov et al., 1995; Castellari et al., 2000; Korres et al., 2000]. This approach is not available to us because we do not know a priori what the SSS was for the Late Miocene (rather, we would like to model it). A freshwater flux was also used by Bigg [1994] in his experiments for the Mediterranean during the Pleistocene.

[15] Of the various fluxes, solar radiation and precipitation are dependent only on factors external to the ocean. The other components, longwave back radiation, sensible heat flux, evaporation and wind stress, are controlled by atmospheric parameters and by the (model-derived) sea surface

temperature (SST). The relevant atmospheric parameters are air temperature, relative humidity, cloudiness, and winds. We use solar radiation and atmospheric parameters computed by Gerasimos Korres of Athens University and made available in the context of the Mediterranean Forecasting System Pilot Project (MFSPP; see http://www.oc.phys.uoa.gr/mfspp). Fields are based on a climatology obtained by averaging of European Centre for Medium-Range Weather Forecasts (ECMWF) re-analysis data for the period January 1979 to December 1993 and have a resolution of $1° × 1°$ (Korres and Lascaratos [2003] give details of the data processing). Solar radiation was computed using the Reed [1977] formula. Precipitation is taken from the work of Jaeger [1976] and is also made available through the MFSPP; the resolution is $5°$ longitude by $2.5°$ latitude.

[16] Solar radiation, precipitation, and the atmospheric parameters are each incorporated in the form of 12 monthly averaged fields assigned to the middle of each month; linear interpolation is used at all other times. The fields are first expanded horizontally to cover all "wet" model cells by fitting a minimum curvature surface to the available data. Then, the fields are fitted to the model grid through bilinear interpolation. Prior to horizontal expansion the central part of the fields is masked out (see Figure 1, middle). This is to prevent a signature of the coasts of present-day Italy and Sicily from showing up in the Late Miocene runs. For the sake of consistency this masking is also done for the present day (where it can be shown to have but a negligible effect on the results). Masking is not necessary or meaningful for the low resolution precipitation fields.

[17] At each time step the model calculates back radiation, sensible heat flux, evaporation, and wind stress from the atmospheric parameters and the modeled SST, and combines these with solar radiation and precipitation to obtain the three net forcing fluxes. Longwave back radiation is computed using the formula of Bignami et al. [1995]. Sensible heat flux, latent heat flux, and wind stress are defined by classical bulk aerodynamic formula using coefficients due to Budyko [1963] and Hellerman and Rosenstein [1983]. Examples of the calculations can be found in the work of Castellari et al. [1998] and Korres and Lascaratos [2003].

[18] Figure 3 illustrates the resulting fluxes for the case that the observed SST [MODB-MED5, Brasseur et al., 1996] is used instead of a modeled distribution of temperature. The basin shows a net cooling in winter and a net heating in summer. Throughout the year, evaporation exceeds precipitation almost everywhere. The wind stress patterns clearly shows the presence of the Alpine mountain ranges with winds being channeled through the gap between the Pyrenees and Alps and across the Aegean Sea.

2.4. River Discharge

[19] Inflow of fresh water from the major rivers is accounted for in simplified fashion by locally increasing the precipitation term of the surface forcing. Discharge is taken constant throughout the year. Included in the present-day run are the Ebro, Rhône, Po, Nile, and the inflow from the Black Sea. Discharge values are from Zavatarelli and Mellor [1995]; for the Nile we use a value of 285 m^3 s^{-1}
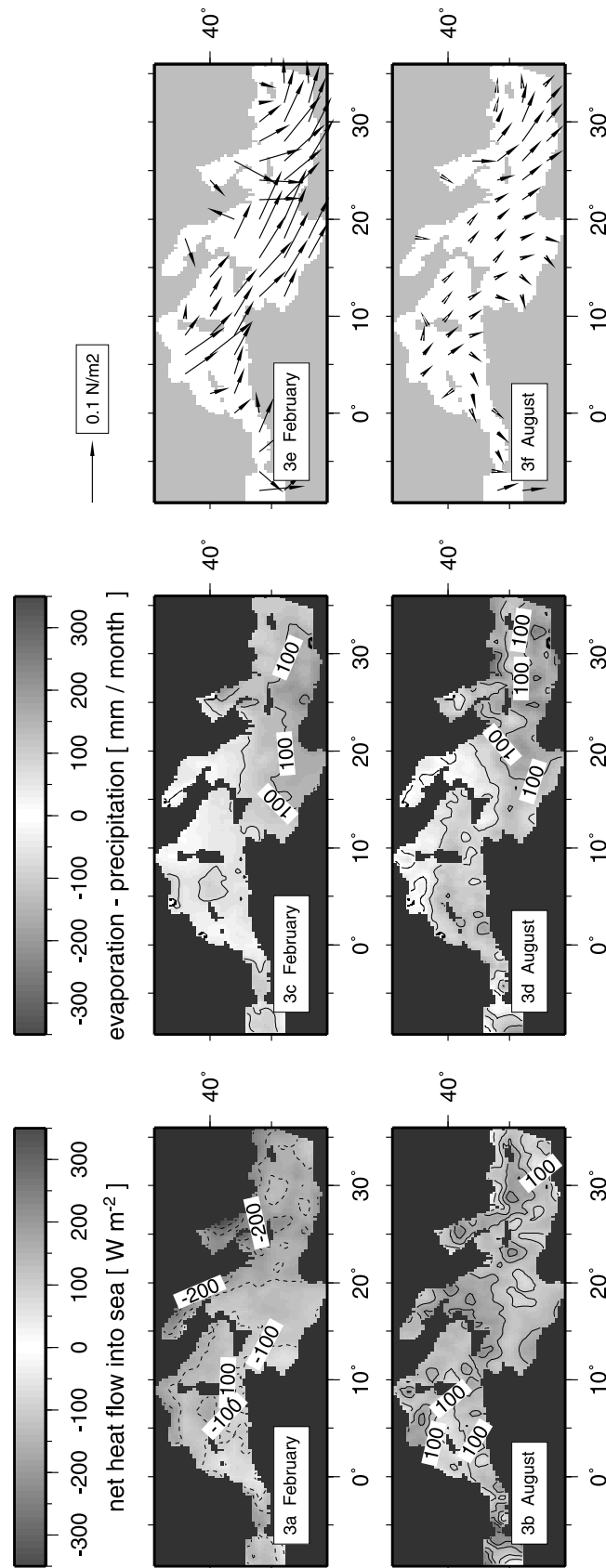
Figure 3. Forcing fluxes found by combination of the atmospheric parameters with the observed SST. (a–d) Gray shading is proportional to absolute magnitude; signature of contour lines indicates whether values are positive (drawn line) or negative (dashed line). (a and b) Net heat flux into the sea in February and August. (c and d) Net freshwater flux in February and August. River discharge is included. (e and f) Wind stress in February and August.
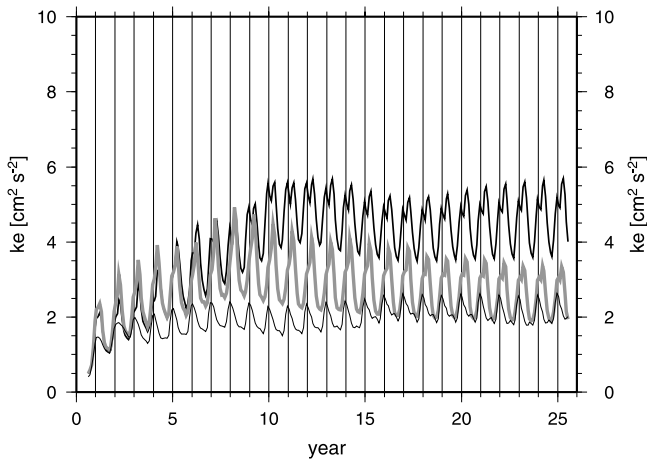
Figure 4. Kinetic energy measure averaged over basin volume as a function of model time for three experiments. Thin line, present-day control; bold line, Late Miocene reference paleorun; shaded line, Late Miocene with deep connection between western and eastern subbasins.

(i.e., 10% of the discharge that existed prior to damming and extraction of water for irrigation; after *Johnson* [1997] and *Bethoux* [1984]). To keep the paleorun identical to the present-day experiment in this respect, the rivers and Parathys/Black Sea outflow are included without change in the Late Miocene experiment. The Po River is positioned in the northwestern corner of the paleo-Adriatic Sea. As explained, inflow from the Parathys/Black Sea is the subject of a separate experiment.

3. Model Analysis

3.1. Present-Day Control Experiment

3.1.1. Average Properties

[20] To monitor the overall intensity of flow in the model we define a kinetic energy measure. Its value at a given time is obtained by averaging over the whole volume of the basin the square of velocity divided by two (i.e., kinetic energy with density divided out). Figure 4 shows how this measure varies with time for the control experiment. In the calculation of all volume averages the "basin" is taken to start at the eastern end of the model representation of the Strait of Gibraltar. We find that by about year 6 or 7 of the integration the model has reached a more or less steady annual cycle. The maximum in energy occurs in December, the minimum at the end of September. The peak coincides with the maximum in applied wind stress. The minimum occurs at the end of the summer season with low winds and represents a time at which the density structure is stable due to summer heating.

[21] The evolution of average temperature and salinity is illustrated by Figure 5. Curves are shown for the entire basin and for the western and eastern subbasin separately. Regarding temperature it appears that the western Mediterranean basin (WMed) stabilizes. However, it does so at a value that is about 0.3°C above the observed annual mean of 13.4°C. The curve for the eastern Mediterranean basin

(EMed), and hence that for the entire basin, shows a steady increase. The temperature drift of the whole basin amounts to approximately 0.02°C yr^{-1}. For comparison, the observed annual mean temperature of the EMed is 14.2°C. In terms of salinity we observe a similar behavior of the subbasins. The WMed settles at a salinity that is close to the observed value of 38.4 psu. Salinity of the EMed increases steadily. It is the deeper levels that are responsible for the remaining drift, as can be seen when salinity is viewed layer by layer rather than for a whole (sub) basin (Figure 6).

[22] Basin averages of temperature and salinity have also been examined for a longer run lasting 125 years (not shown). Near the end of this period the average temperature seems to settle to a maximum value. Salinity, however, keeps increasing at a rate that only slightly decreases with time.

[23] A final overall property that must be considered concerns the air-sea fluxes. For the middle of each month of year 15 of the control run we average the atmospheric fluxes over the surface area of the model. The resulting curves are shown in Figure 7 together with the curves that we obtain when, rather than the modeled sea surface temperature (SST), we use the observed monthly mean
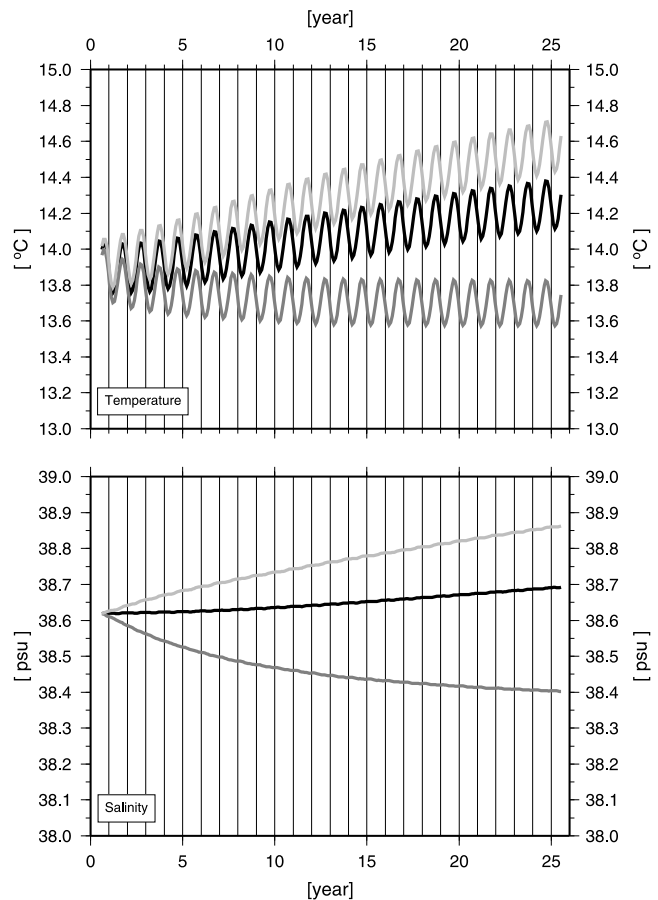

Figure 5. Volume-averaged temperature and salinity as a function of model time. Present-day control experiment. Black line, whole basin; dark shaded line, WMed; light shaded line, EMed.
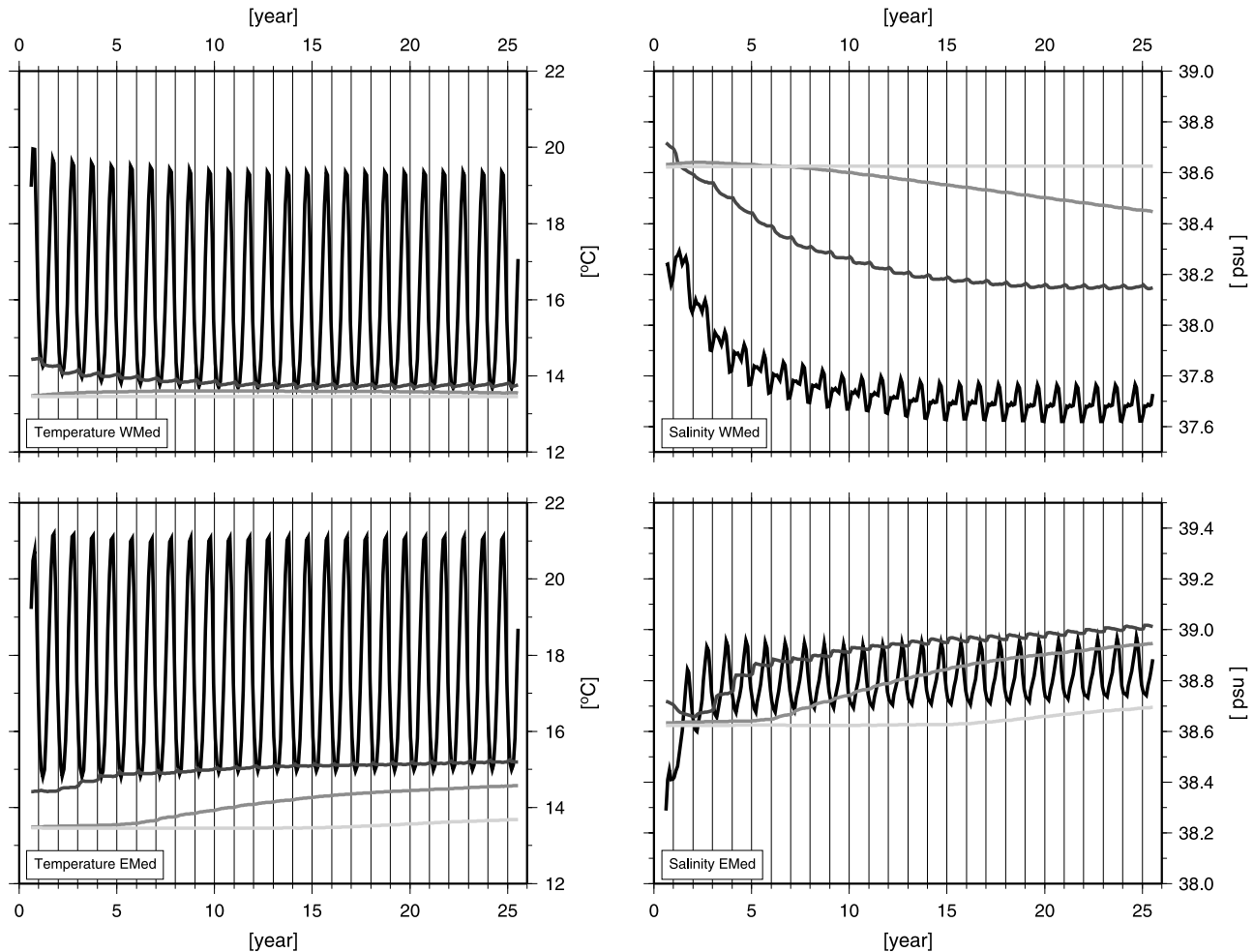
Figure 6. Evolution of layer-averaged temperature and salinity for the (left) WMed and (right) EMed. Present-day control experiment. Ever lighter shading corresponds to ever deeper layer. Temperature is shown for layers at 30, 280, 850, and 2750 m. The topmost layer for which salinity is shown is for 5 m; other layers as for temperature.

temperature to calculate the fluxes. Figure 7 also states the annual budgets for each case. Surface-averaged wind stress during year 15 proves nearly identical to that corresponding to the observed SST. The net surface freshwater flux (including the river discharge) differs in particular in autumn and winter when year 15 of the model run shows less net evaporation. Since precipitation is not affected by modeled SST this lower net evaporation may simply be taken to imply lower evaporation. In summer the modeled evaporation is somewhat higher than that "observed." On an annual basis the net freshwater loss during year 15 is slightly less than observed. Linked to the freshwater flow through the flux in latent heat, the curve for total heat flow shows somewhat less cooling, corresponding to less evaporation, in fall and winter. The reverse is true for summer. As a whole, year 15 is found to involve a net cooling through the sea surface that is lower than observed. This under representation of cooling may well "explain" the temperature drift already reported. It is easily shown that a net surface flow of 1 W m^{-2} into the sea results in a temperature increase of 0.005°C yr^{-1}. Thus the difference

between actual and model-derived net heat flux on the one hand, and the temperature drift on the other, are of the correct order of magnitude to be causally related. Note that in this calculation we ignore changes in the heat content of the basin due to the exchange of water with the Atlantic Ocean.

3.1.2. Horizontal Flow

[24] In an overall sense the model-predicted surface flow is in fair correspondence with the observed pattern [see, e.g., *Pinardi and Masetti*, 2000]. Figure 8a illustrates the mean surface flow (30 m depth) during year 15 of the integration. All annual mean fields presented here have been computed from 12 velocity fields sampled at the middle of each month. Closer sampling was found not to change the resulting mean. Inflow of water from the Atlantic Ocean can be followed through the Sicily Strait, all the way into the easternmost Levantine basin. Here the flow turns back westward around the island of Cyprus. In the northern part of the western Mediterranean a cyclonic gyre is present: the model representation of the Gulf of Lions gyre. The Tyrrhenian Sea is occupied by a northward flow branching off
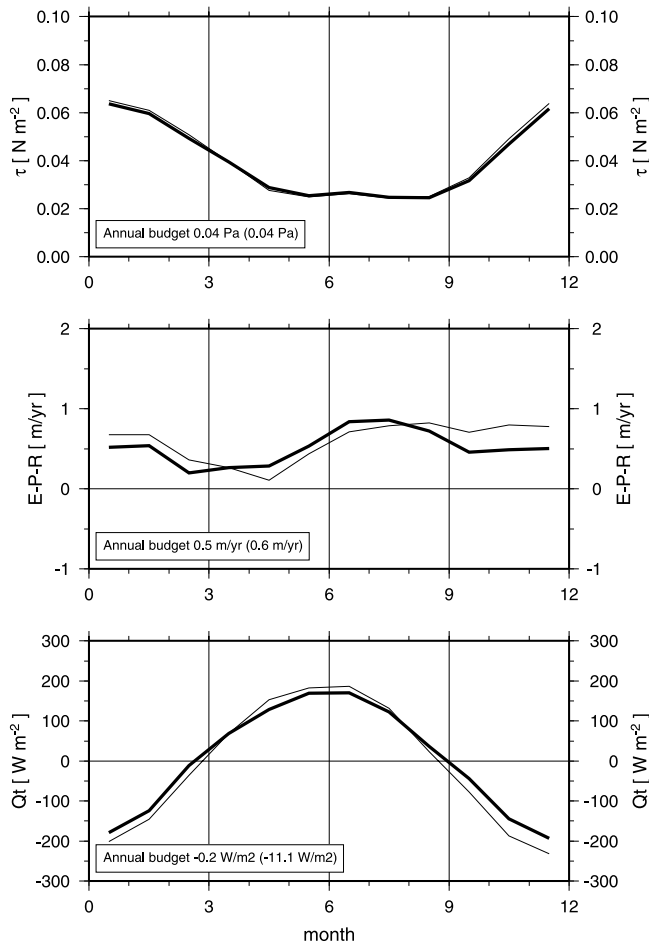
Figure 7. Variation of basin-averaged surface fluxes during year 15 of the control experiment (bold lines) and as found using observed SST instead (thin lines). Annual budgets are also given; values in parentheses refer to the case with observed SST. The contribution from rivers, kept constant with time, has been included.

from the Atlantic stream. In the northern Ionian basin a clear cyclonic gyre can be observed. The flow pattern is complex in the Ionian basin south of the Atlantic stream. The only notable mismatch concerns the location of the Atlantic inflow in the WMed: unlike the model predictions, this flow is observed to stay south of the Balearic islands.

[25] At a depth of 280 m, just above the sills at Gibraltar and Sicily, both straits show the expected westward flow, opposite to the flow at shallower levels (Figure 8b). Flow in the eastern Mediterranean partly mimics the surface flow albeit at much lower velocity. The model does not show a westward flow that passes south of Crete and originates in the area where in reality one observes the formation of Levantine Intermediate Water (between Crete and Cyprus). Instead, the model has a westward flow through the southern Aegean Sea that does not connect directly with the westward flow through the Strait of Sicily. This lack of a direct flow from the Levantine into the WMed could be one

of the factors contributing to the unrealistic steady increase in salinity of the EMed.

[26] The model predicts an annual mean volume transport (one way) through the Strait of Gibraltar of 0.8 Sv. This value is on the low side of the range inferred for the actual transport: 0.7 Sv based on current measurements [*Bryden and Kinder*, 1991] and 0.8–1.6 Sv based on a consideration of the water and salt budget of the whole basin [*Bethoux et al.*, 1999]. The transport we find for the Strait of Sicily, 1.1 Sv, is slightly lower than the observed value of 1.2 Sv, reported by *Bethoux and Gentili* [1999].

3.1.3. Thermohaline Circulation

[27] In order to assess how well the model reproduces the thermohaline circulation we first focus on the distribution of salinity. Salinity shows much less seasonal variation at the upper levels than temperature and forms a good tracer of water masses. We will again consider year 15 of the integration at which time the salinity structure of the deeper parts is still close to the initial situation and the main features of the thermohaline circulation are well displayed. At the surface (5 m depth) the annual mean salinity pattern clearly shows the relatively fresh inflow of Atlantic water, in the WMed as well as in the EMed (Figure 9a). The result of net evaporation is obvious in the raised salinity of the EMed. The presence of rivers is expressed by locally strongly reduced salinities. The expression of the Nile is notably subdued, in accordance with the available climatological data (MODB; *Brasseur et al.* [1996]). The modeled SSS differs from the observed field in the northward shifted Atlantic inflow and in its high salinity in the southern Ionian basin. The horizontal slice at 280 m (Figure 9b) captures the upper part of the outflow of salty water from the EMed into the WMed. This outflow is centered at a depth of around 500 m.

[28] The high salinity waters at 280 m in the southern Aegean Sea and between Crete and Cyprus and further north, are placed at this level by vertical mixing during February and March and may be considered the model representation of intermediate water formation. From depths of around 300 m just west of Cyprus, mixing increases in depth going west and reaches down to about 900 m in the southern Aegean Sea. In the southwestern Aegean Sea mixing extends down to the seafloor. Also immediately to the south of Crete mixing reaches about 500 m. Figure 9b shows how the salty outflow from the Aegean Sea can be followed in westward direction. Salinity sections through the WMed show a mostly still horizontally stratified structure apart from the outflow from the EMed. In both the northern Tyrrhenian Sea and the Gulf of Lions does the model show deeper mixing, down to 300–400 m.

[29] In reality, intermediate water formation is thought to be restricted to the area of the Rhodes gyre, to the ESE of Crete; the Aegean Sea is known to currently produce deep water. Although our model does indeed show intermediate depth mixing in the area between Crete and Cyprus and near complete mixing in the southern Aegean Sea, it appears to overestimate the areal extent of that mixing. Moreover, the model does not reproduce outflow of deep water from the Adriatic Sea to the bottom of the EMed, nor the formation of deep water in the Gulf of Lions area.
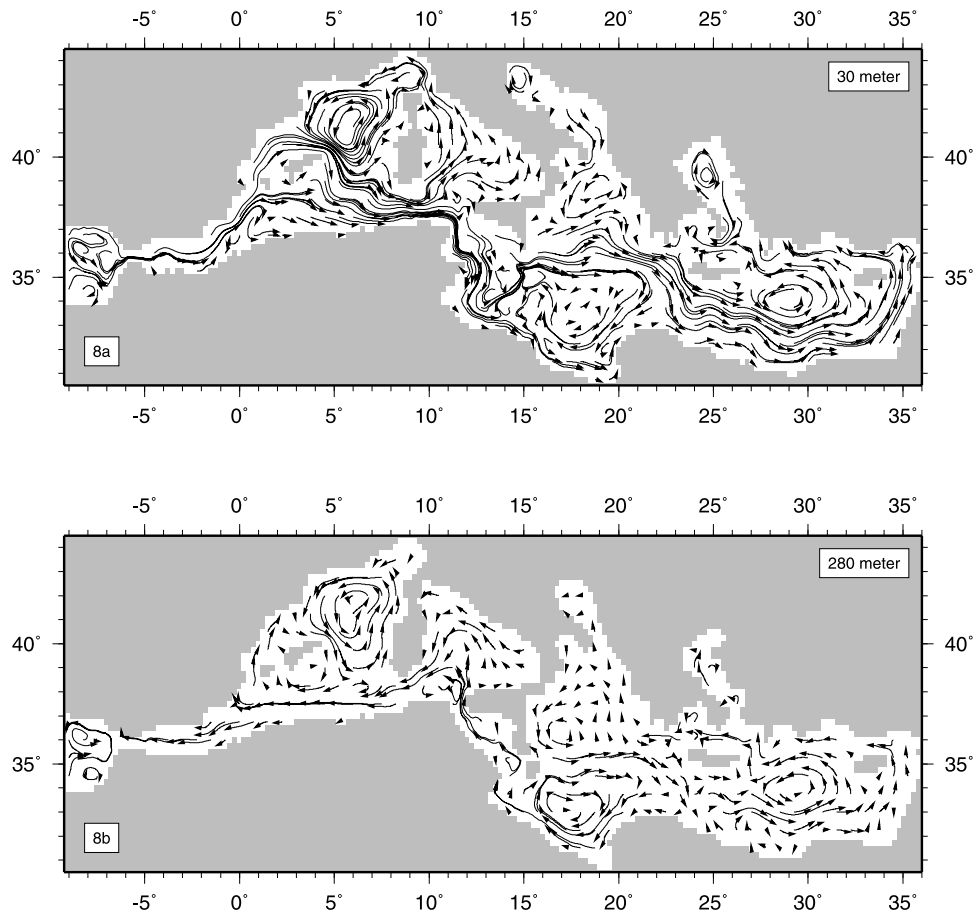
Figure 8. Trajectories of horizontal flow at two depths, 30 and 280 m; mean of year 15 of the control experiment. Shown are the paths particles would travel in 60 days keeping the annual mean velocity field constant.

[30] To support our remarks concerning the simulated thermohaline circulation we show in Figure 10 the zonal overturning stream function for year 15. This stream function was calculated on the basis of the annual mean velocity field following the definition of *Stratford et al.* [2000]. At each longitude and depth, velocities are integrated in the meridional direction thus obscuring any north-south variation that may be present. The resulting graph is potentially as misleading as it is revealing and must be interpreted with caution. Note in particular the central portion of Figure 10 where flow in the eastern Tyrrhenian Sea is combined with flow in the northernmost Adriatic and to the south of Sicily. The reason for this being of course that these areas share the same longitude. Notwithstanding these distortions the figure clearly demonstrates the presence of overall eastward transport at the surface in both basins and a westward return flow at intermediate depth. The latter is displaced downwards in the area west of Crete due to the outflow of dense water from the southern Aegean Sea. Demonstrated very clearly by Figure 10 is the failure of the control experiment to simulate circulation at depths below the intermediate return flow.

[31] In summary, the present-day control experiment tells us that model predictions of the surface to intermediate depth circulation and water properties are reasonably accu-

rate with the chosen set up (in particular: grid resolution and type and frequency of atmospheric forcing). Deep circulation is not well simulated however, and, probably as a result of this, the model does not reach constant basin-averaged temperature and salinity. We are thus restricted to runs that are relatively short because the basin overturn time is about 100 years.

3.2. Late Miocene Paleogeography (Reference Paleorun)

3.2.1. Average Properties

[32] Surprisingly, the basin-average kinetic energy is higher and the annual cycle is different for a Late Miocene paleogeography (Figure 4). During the first 10 years the kinetic energy steadily increases; following this period it varies much less but is still subject to slow changes in its annual cycle and range. Instead of one maximum in December there are now two peaks, one in December, the other in March/April. As we will see in detail below, the increase in kinetic energy compared with the control run is due to more intense horizontal flow at surface and intermediate depths, more widespread vertical mixing (most likely responsible for the March/April peak) and the presence of significant flow at deeper levels also.
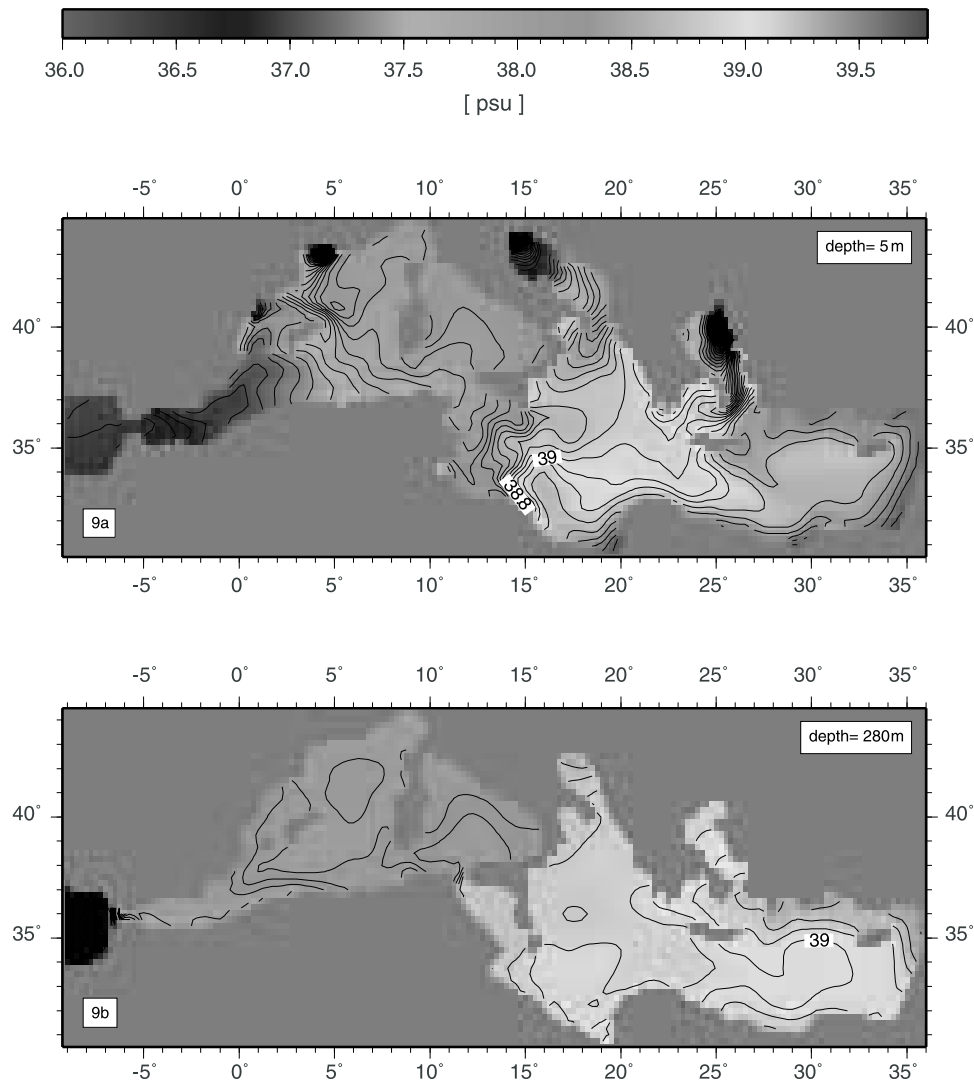
Figure 9. Horizontal slices through the modeled salinity field at the surface (5 m) and at 280 m; mean of year 15 of the control experiment. Land area is gray; black indicates salinity below 36 psu (due to rivers). Contour interval is 0.1 psu. See color version of this figure at back of this issue.

[33] Drift of basin-averaged temperature is less than in the control run (compare Figure 11 to Figure 5). This is caused by a much weaker increase in temperature of the EMed. Also, in contrast to the control run, we now find an initial period of stable temperature in the EMed. In the WMed temperature evolves similarly in both runs. Regarding salinity it is the WMed that is different from the control case: salinity decreases faster initially and seems to settle sooner. This behavior of the WMed results in a stronger drift of the basin average. As was found for the control experiment, the temperature and salinity of the upper layers do reach a steady state after several years of integration and it is the deeper levels that cause the remaining drift (not shown). For the case of a 125 year integration, basin-averaged temperature and salinity are found to behave in a similar way as in the control experiment: temperature appears to settle while salinity keeps increasing.

[34] In light of these differences in circulation intensity, temperature and salinity, one might expect the surface average air-sea fluxes to be different. But air-sea fluxes for year 15 of the paleorun (not shown) generally stay close to the corresponding curves of the control experiment although the annual heat budget is now found to be slightly positive with a small net flow of heat from the atmosphere into the basin (0.8 Wm^{-2}) rather than a minor cooling.

[35] It is not straightforward to explain the response of basin-averaged temperature and salinity to the imposed change in geometry. The close similarity of air-sea fluxes for control and paleorun implies that sea surface temperatures are the same throughout the year in both experiments. This is easily checked to indeed hold true and it shows us exactly what the applied atmospheric forcing amounts to: essentially the same sea surface temperature pattern through time, independent of assumed basin geometry. It also means that the different evolution of basin-average temperature in
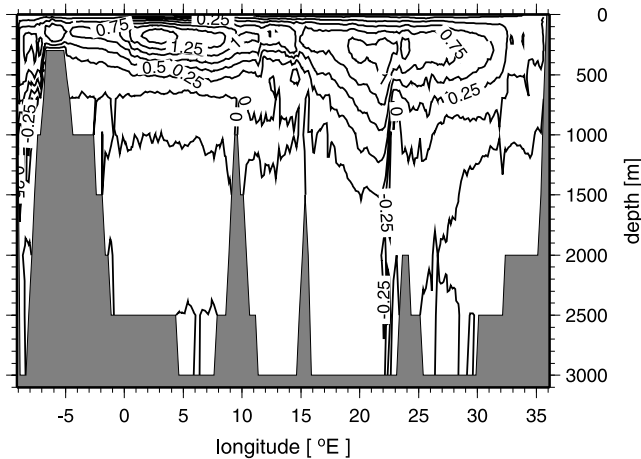
Figure 10. Zonal overturning stream function calculated on the basis of the annual mean velocity field of year 15 of the control experiment. Contour interval is 0.25 Sv. Indicated at each longitude is the most deeply situated seafloor. Transport is along streamlines to the right when going from high to low values of the stream function.

the EMed must have its origins at depth and is due either to changes in exchange with the WMed or to different vertical mixing in the basin itself. Remarkably, if these inferences are correct, the different exchange and/or mixing does apparently not affect the average salinity of the EMed. In the WMed the different evolution of salinity is likely to reflect a change in exchange with the Atlantic Ocean while the temperature at surface and deeper levels remains the same.

3.2.2. Horizontal Flow

[36] The mean surface flow during year 15 of the Late Miocene experiment is shown in Figure 12a. Both gateways to the Atlantic show a surface inflow. Inflow through the Betic gateway of the southern Iberian peninsula turns around the Balearic islands and is joined by the inflow through the Moroccan gateway of northwestern Africa before entering the EMed through the strait south of the Corsica-Sardinia block. Just east of the point where the coast of northern Africa turns abruptly south, the Atlantic stream bifurcates. One branch hugs the African coast while the northern branch passes along an intense cyclone and can be traced into a cyclonic circulation in the easternmost basin. Flow in much of the eastern basin is rather complex. An elongated anticyclonic gyre is present over the Apenninic foredeep. At 280 m depth the straits connecting the EMed to the WMed and the WMed to the Atlantic all show westward flow. Exchange at the straits is thus similar in nature to the present-day situation. Annual mean eastward volume transport in both the Betic and the Moroccan gateway amounts to 0.5 Sv. The outflow proves to be partitioned, however. Westward return flow in the Betic gateway is found at 0.3 Sv while the Moroccan gateway has 0.7 Sv. Combined, the two gateways acccomodate a volume transport that is somewhat larger than the value found for the control experiment (0.8 Sv). For the strait south of the Corsica-Sardinia block we find a transport of 1.2 Sv, close

to the value found for the Strait of Sicily in the control case (1.1 Sv).

[37] The intense gyre in the central Ionian basin (near 39°N, 16°E) can be shown to extend down to the seafloor. Its location is controlled by bathymetry; as can be seen in Figure 12b the gyre occupies the deep "channel" between the Sicily platform and Apulian platform. The gyre appears to be the result of a confluence of 3 flows in the depth interval between about 280–500 m: an eastward flow along the adjacent segment of African coast, a northward flow coming from the south along the African coast east of 15°E, and a westward flow just off the Apulian platform. Several dedicated sensitivity experiments have shown the gyre is strengthened by, but not a consequence of, the applied winds. Also, when the model bathymetry is smoothened, thereby reducing the steepness of the flanks of the Ionian channel, the gyre becomes less concentrated which confirms the constraining role of bathymetry. Indeed, in the extreme case that the Sicily platform is taken not to exist, the gyre disappears and flow in the EMed becomes completely different.

3.2.3. Thermohaline Circulation

[38] The salinity field at 5 m (mean of year 15; Figure 13a) distinctly shows the inflow of Atlantic water into the WMed and its relatively fresh continuation into the EMed.
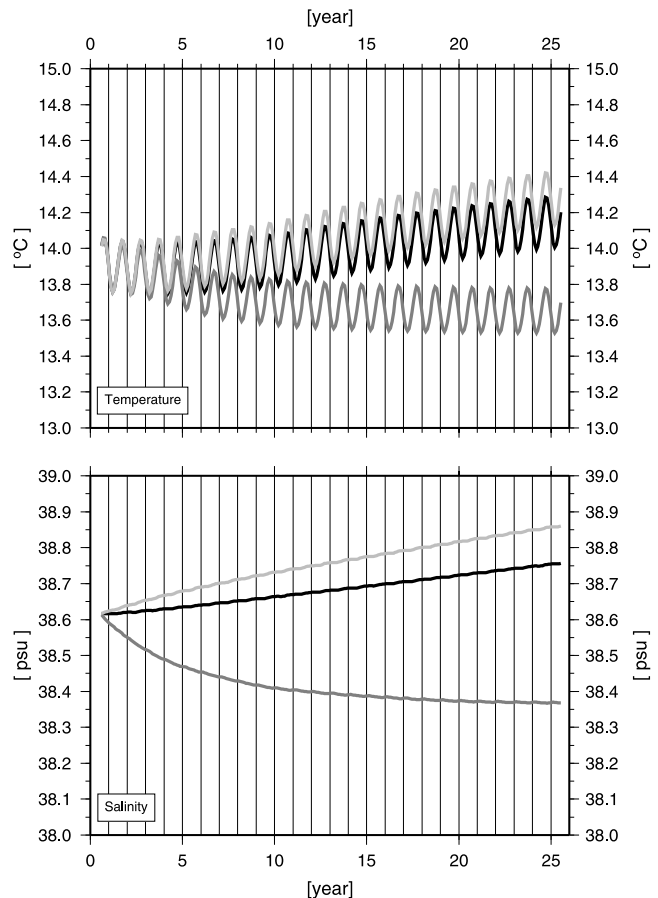

Figure 11. Volume-averaged temperature and salinity as a function of model time. Late Miocene experiment (reference paleorun). Black line, whole basin; dark shaded line, WMed; light shaded line, EMed.
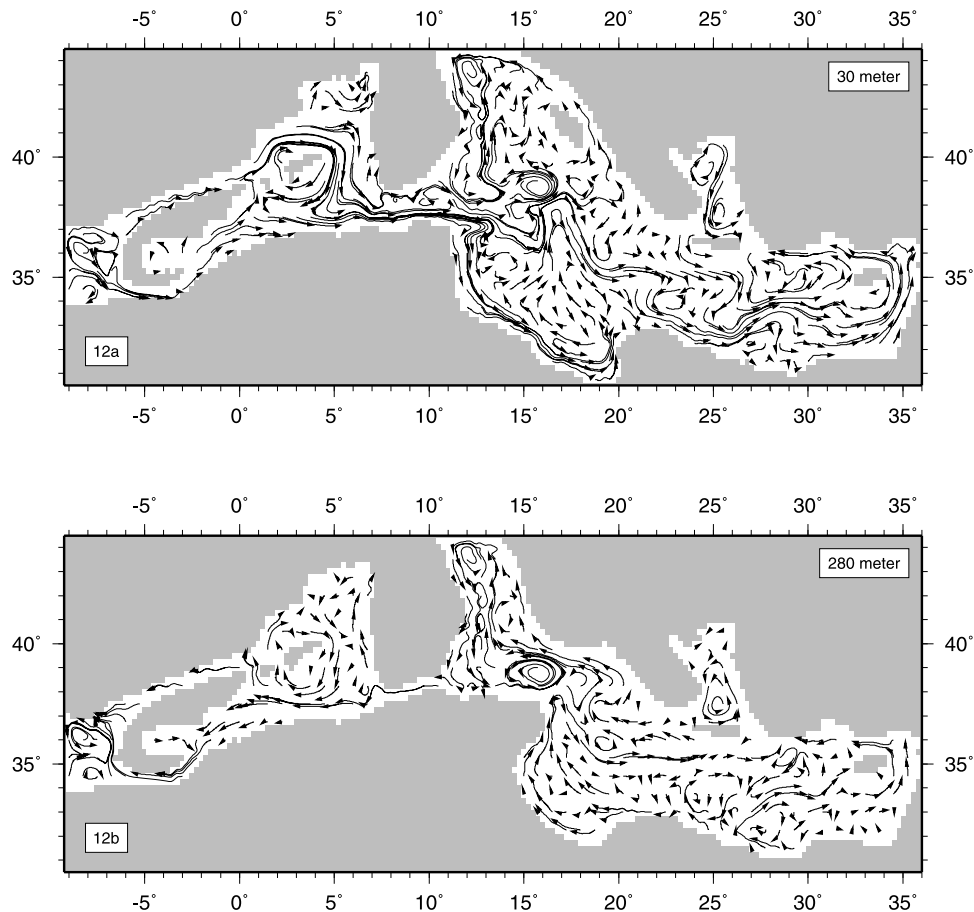
Figure 12. Trajectories of horizontal flow at two depths, 30 and 280 m; mean of year 15 of the Late Miocene experiment (reference paleorun); 60 day trajectories.

As in the control run much of the Levantine basin is characterized by high salinity. In contrast to the present-day experiment, we now find the fresh water from the Paratethys/Black Sea to extend well outside of the Aegean Sea. At present, the water from the Black Sea is contained in the northern Aegean Sea by a strong westward flow through the southern Aegean Sea. In the past, the Hellenic arc was less strongly curved and the model suggests this prevented such throughflow, allowing the Paratethys water to reach the Levantine basin. The outflow from the Aegean Sea has the effect to block vertical mixing in the area near Crete as can be learned from the slice at 280 m which shows high salinity water, brought to this depth by winter mixing, only to the east of Crete (compare Figures 13b and 9b). The northern part of the Levantine basin is again a site of intermediate depth winter mixing. As is clear even from the annual mean fields of Figure 13, the Adriatic basin is now found to be of nearly homogeneous salinity. In fact, vertical slices through the Adriatic in February and March reveal not only this well-mixed nature but also show water to flow out of the basin at depth, into the adjacent portions of the EMed (Figure 14). This feature of the modeled Late Miocene circulation, in stark contrast with the control run, is well brought out by the mean zonal overturning stream function of Figure 15. Apart from the surface/intermediate

depth cell of circulation we now clearly observe a deeper cell in the EMed. This deeper cell would appear to be triggered by the outflow of dense water from the Adriatic. In the WMed no deep circulation is predicted. Note that in the case of the Late Miocene, basin geometry is such that the stream function does not involve a distortion in its central portion, all of the EMed lying east of all of the WMed. The robustness of the deep circulation cell has been assessed by computing the stream function also after an additional 100 years of integration (not shown). At year 115 the deep cell is still present and the total transport is only slightly reduced.

3.3. Role of Forcing Over Atlantic Gateways

[39] In the reference paleorun described above, there was no forcing over the Betic and Moroccan gateways. The reason for this is clear: these gateways are dry land at present and are not included in the oceanic databases for the Mediterranean. As an alternative we briefly describe (without illustrations) an experiment in which the forcing over these parts follows from interpolation. To this extent we fit a minimum curvature surface to the data we do have, including data from the Atlantic west of Gibraltar and just off the west coast of the Iberian peninsula.

[40] With forcing over the gateways included, the salinity drift of the EMed increases; the WMed settles at a value that
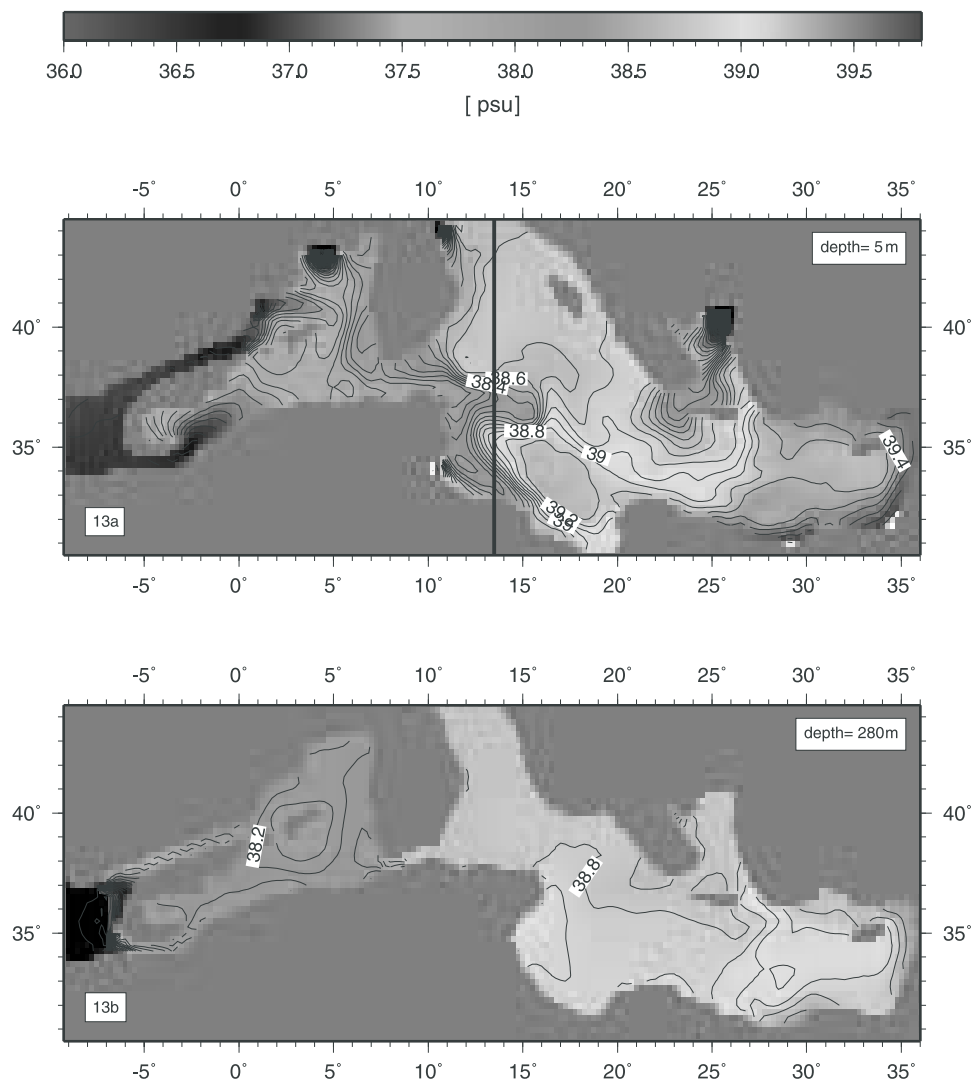
Figure 13. Horizontal salinity fields at the surface and 280 m; Late Miocene experiment (reference paleorun). Annual mean of year 15. Contour interval is 0.1 psu. Bold line indicates section of Figure 14. See color version of this figure at back of this issue.

is somewhat higher than without gateway forcing. The evolution of basin-averaged temperature drift is hardly changed. In terms of the flow field the most striking difference concerns the gateways themselves. For example at 30 m depth, flow traces are found to converge to points at the south coast of the gateways; there no longer is direct through-flow as in Figure 12. Within the Mediterranean basin the flow field is very similar to that found before. The surface salinity field now shows a stronger salinity increase over the length of the gateway (hence the change in flow): once it has arrived in the WMed the Atlantic water is less fresh. This increase in salt content of the inflow from the Atlantic is expressed in the salinity of the inflow into the EMed as well. Salinities are found to *decrease* in the area of winter mixing in the northern Levantine. This is due to the fact that mixing now extends somewhat deeper than before and more subsurface water, in this area of relatively low salinity, is taken up into the mixed column. In terms of the mean zonal overturning stream function the main effect of
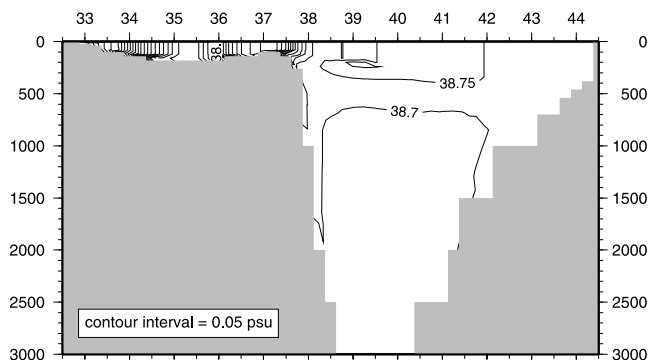

Figure 14. Vertical north-south section through the salinity distribution of the past Adriatic Sea (reference paleorun). Line of section is shown in Figure 13. Mid-February of year 15. Contour interval is 0.05 psu.
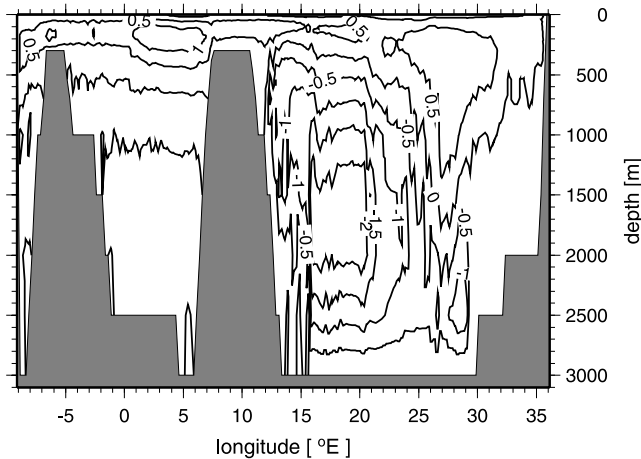
Figure 15. Zonal overturning stream function calculated on the basis of the annual mean velocity field of year 15 of the reference paleorun. Contour interval is twice that of Figure 10: 0.5 Sv. See caption to Figure 10 for further explanation.

introducing forcing over the gateways is a strengthening of the deep convection cell in the EMed. The increase in depth of winter mixing and in strength of the deep cell in the EMed is a direct consequence of the presence of denser surface waters, now that salinity of the Atlantic water is forced to increase before it reaches the Mediterranean basin.

3.4. Paleogeographical Alternatives
3.4.1. Without Aegean Sea Basin and "Paratethys" Outflow

[41] The evolution of the overall properties (as compared to the reference paleorun) are little affected when the Aegean Sea is represented as dry land and we assume there is no water from the Paratethys entering the EMed. Absence of fresh water from the Paratethys causes a faster salinity rise in the EMed, but salinity drift in the WMed and the temperature behavior of both subbasins remain unchanged. In the surface flow pattern we now miss the outflow from the Aegean Sea and, as a consequence, salinity is increased in the part of the Ionian basin southwest of where the Aegean Sea would be (Figure 16). This same area now proves subject to intermediate depth mixing in February and March. The mean zonal overturning stream function is not much different from that found for the reference paleorun.

3.4.2. Shallow Straits Across the Corsica-Sardinia Block

[42] Paleogeographical constraints do not preclude shallow straits that establish a connection between the WMed and EMed across the Corsica-Sardinia block. Therefore simulations were conducted with two simple east-west oriented channels of 100 m uniform depth (see land mask in Figure 17). While we find essentially the same overall properties as for the reference paleorun, it is interesting to observe the flow in the newly introduced channels. The northern channel shows a westward flow; the southern channel has eastward flow (Figure 17). In both channels the sense of flow is uniform with depth. Flow in the

channels appears to be a logical continuation of the flow pattern in the adjacent basins: the reference paleorun shows westward flow in the Adriatic just east of the northern channel and eastward flow in the WMed west of the southern channel (Figure 12a). Channel flow appears mostly wind-driven. When the experiment is repeated without applied winds, channel flow nearly disappears while the overall temperature and salinity variation across the Corsica-Sardinia block is still the same as in the case including winds. Finally one may notice in Figure 17 how introduction of the channels affects flow in the WMed.

[43] Changes in the salinity distribution as a result of these channels prove rather complex. Apart from the expected reduction of salinity where the southern channel empties into the EMed, there are other reductions and also areas of salinity increase that reflect changes in the overall flow pattern and consequent vertical mixing. Salinity changes were found to occur in the range of -0.5 psu to $+0.5$ psu. All salinity changes are restricted to the basin west of about longitude 15°E: most of the Ionian and all of the Levantine basin are not affected. The mean zonal overturning stream function displays only minor changes.

3.4.3. Deep Connection Between Western and Eastern Mediterranean

[44] Uncertainty regarding the depth of the strait that connected the two main subbasins in the Late Miocene has motivated our last experiment. The sill south of the Corsica-Sardinia block is lowered to 1000 m. Again, this value is chosen somewhat arbitrarily. For comparison, at present the passage between Sardinia and Africa reaches $1300-1400$ m at its deepest point. The evolution of kinetic energy that we find for this experiment is included in Figure 4. As for the standard paleorun kinetic energy initially increases, but following year $8-9$ the curves diverge and our new run settles at a lower value. Also, more than in any of the other experiments we have presented, the annual cycle still changes after year 15. Concerning the evolution of average temperature and salinity, it is the latter property in particular that behaves differently. The WMed settles sooner and at a higher (i.e., less decreased) salinity. The EMed shows a reduced salinity increase.

[45] The essential change in the surface flow pattern is an increase in speed and width of the Atlantic inflow and its continuation into the EMed. Indeed, as demonstrated by the mean zonal overturning stream function of Figure 18, we now find the entire surface/intermediate circulation cell to have intensified. The return branch at intermediate depth moves down to occupy the extra space provided by the deeper connection between the two subbasins. In contrast, the deeper cell in the EMed is reduced in strength.

[46] The response of the two main modeled circulation cells appears to be related by the salinity of the Adriatic Sea. There, as a direct consequence of the intensified inflow of Atlantic water, salinity is found to decrease. In turn, this salinity decrease reduces the production of dense deep water, which is what drives the deep cell in the EMed. Our interpretation of the model results is confirmed when we consider the situation 10 years later, i.e., during year 25 of the model run. Figure 4 shows that the peak in kinetic energy in March/April, which reflects the occurrence of
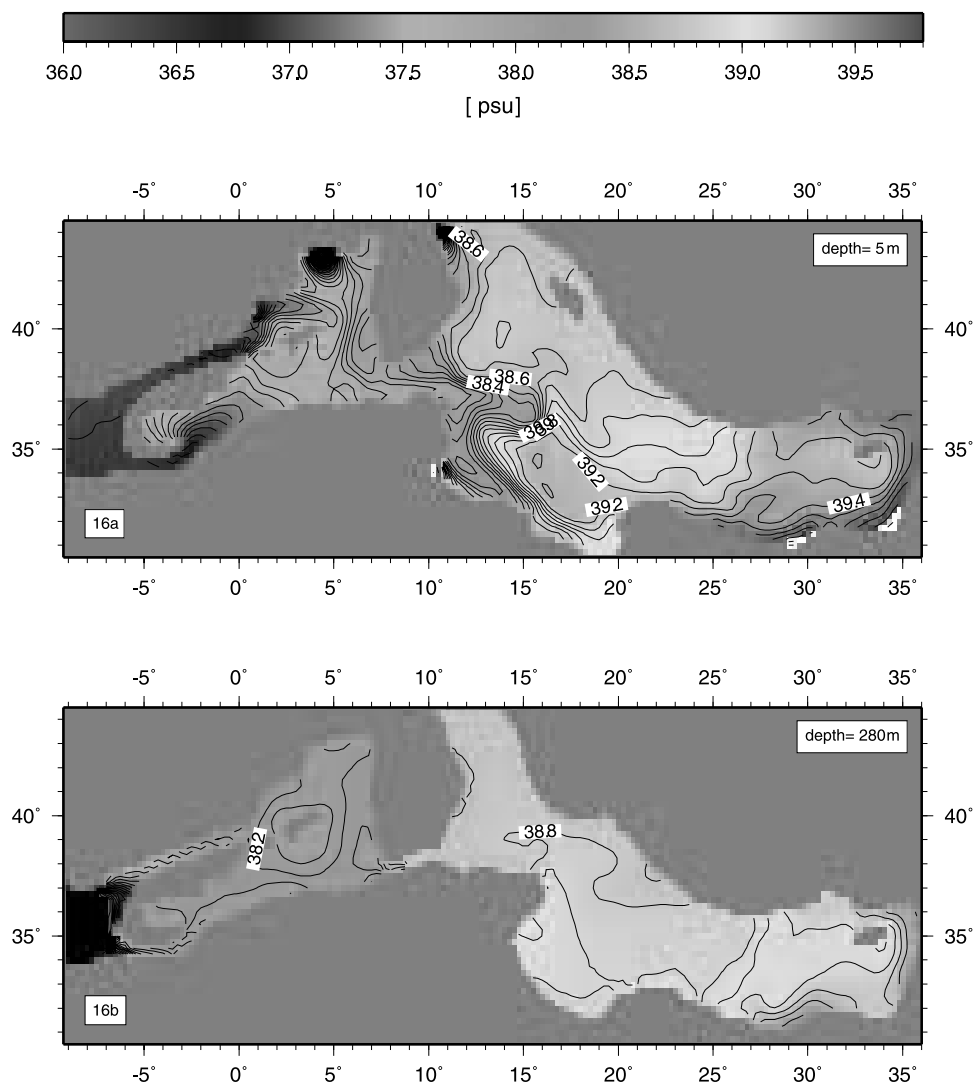
Figure 16. Horizontal salinity fields at the surface and 280 m; Late Miocene experiment without Aegean Sea. Annual mean year 15. Contour interval is 0.1 psu. See color version of this figure at back of this issue.

deep mixing, is much reduced during these extra 10 years. As expected given our interpretation, the corresponding mean zonal overturning stream function shows the deeper cell to have decreased in importance even further.

4. Discussion

4.1. Limitations

[47] Our present-day control experiment is not able to reproduce the formation of deep water, observed to happen in the Gulf of Lions and the southern Adriatic Sea. It is probably for this reason that the model does not reach a steady state in terms of average temperature and salinity. The lack of deep water formation has prompted us to limit the runs to 25 years, about one quarter of the basin overturn time. In these 25 years the upper/intermediate levels of the basin do reach steady state. Nevertheless, the control run reveals a shortcoming of the model that forms a source of

uncertainty regarding the outcome of the paleoexperiments. There are 2 closely related aspects of this uncertainty: (1) as we do for the present day we may be missing sites of deep water formation for the Late Miocene, and (2) since we are limited to short runs the model cannot approach the actual past deep water properties when these were significantly different from the initial (i.e., present-day) conditions.

[48] It is important to point out that our problems with the simulation of deep water formation in the Mediterranean are shared in published studies with similar spatial resolution and frequency and type of atmospheric forcing [e.g., *Bigg*, 1994; *Zavatarelli and Mellor*, 1995; *Castellari et al.*, 2000; *Korres et al.*, 2000]. To make things worse, in view of the questions we set out to answer, we could not resort to using a relaxation to sea surface salinity to circumvent the poor quality of the precipitation data. Of all published models for the present-day circulation, only that developed at University of Edinburgh is exploited on the timescale of the basin
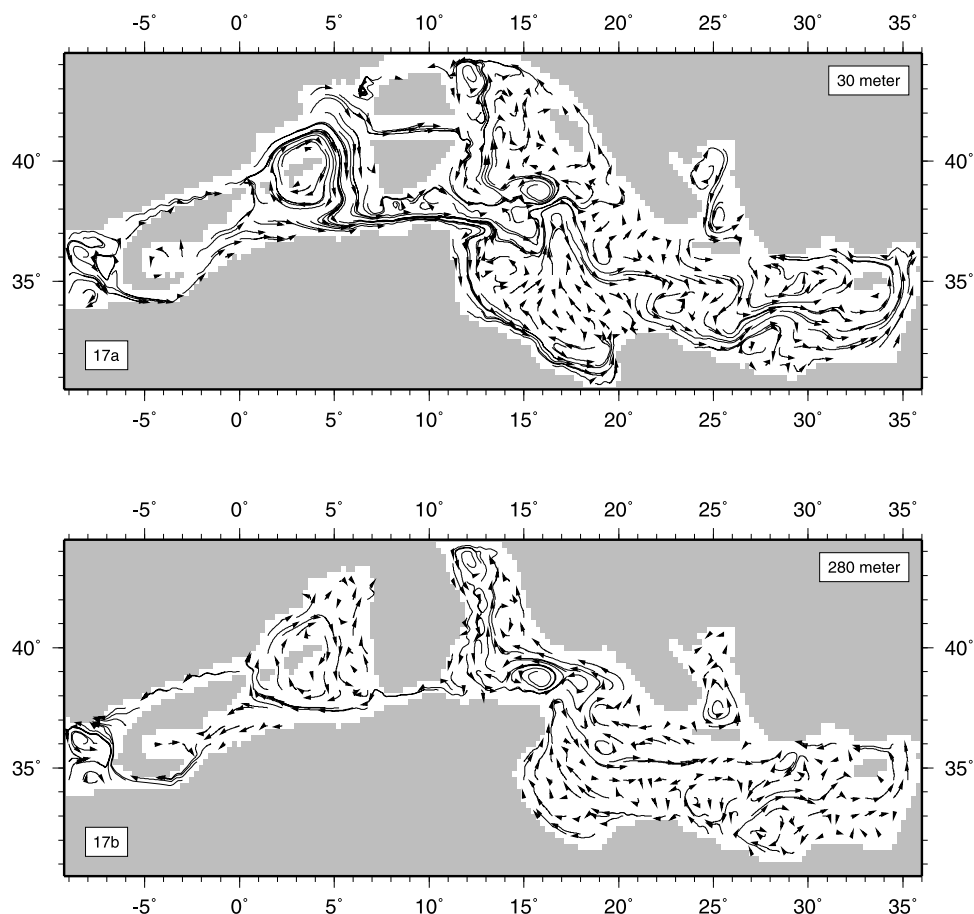
Figure 17. Trajectories of horizontal flow at two depths, 30 and 280 m; mean of year 15 of the Late Miocene experiment with shallow straits crossing the Corsica-Sardinia block. 60 day trajectories.

overturn time, about 100 years [*Wu and Haines*, 1998]. This model does simulate the complete thermohaline circulation but uses either relaxation surface boundary conditions for both temperature and salinity or fluxes that are diagnosed from a previous relaxation run [*Myers and Haines*, 2000; *Myers*, 2002].

4.2. Implications

[49] Notwithstanding the apparent limitations of the model, we feel our results provide fundamental insights into the effects of paleogeography on Mediterranean circulation.

[50] 1. Late Miocene paleogeography creates an upper/intermediate depth east-west cell of circulation similar to today's circulation. Thus, for example, the distribution of faunas and sediment transport directions recorded in Late Miocene sediments should be similar to today. This provides a direct test of the model results. On the basis of a variety of proxy data, *Kouwenhoven and van der Zwaan* [2004] suggest that the Tortonian Sea also comprised 3 main water masses, as it does at present. This is consistent with the results of our paleoexperiment. It would appear that, in order to disrupt the surface/intermediate cell, we would have to resort to changes in aspects held constant in our
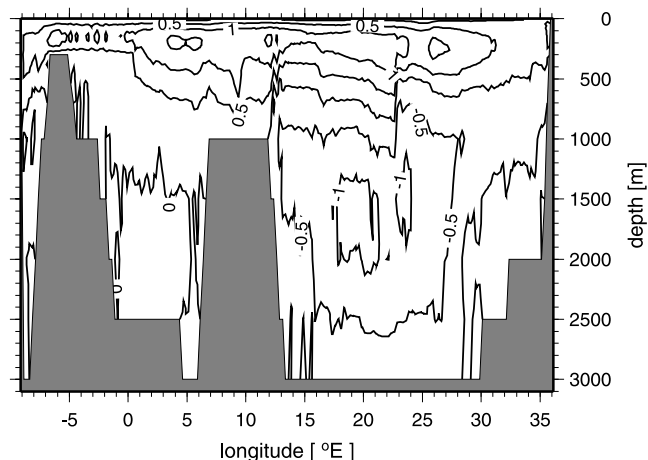

Figure 18. Annual mean zonal overturning stream function for the Late Miocene experiment with deep connection between the western and eastern subbasins. See caption to Figure 10 for further explanation.

modeling so far such as climate and depth of the gateways to the Atlantic.

[51] 2. Late Miocene paleogeography is found to give rise to an intense deep circulation cell in the EMed. This is most likely due to the greater surface area of the Adriatic Sea. Counterclockwise rotation of the Italian peninsula since about 15 Ma was related to opening of the Tyrrhenian Sea at its rear, and resulted in gradual narrowing of the Adriatic, at its front. The Adriatic Sea is situated relatively northward, is subject to strong cooling in winter and collects relatively salty, and hence dense, water from the eastern Mediterranean. These combined factors make it a site of deep water formation in the actual Sea (but this process is not picked up by our control experiment). With the surface area of the Adriatic Sea reconstructed to the Late Miocene situation, water travels a longer path in this region and is thus exposed to the cold atmosphere for a longer time. Consequently, the volumes of water involved in deep mixing increase and the area becomes a site of deep water formation in our paleorun. This particular result may have bearing on the important issue of sapropel formation. If anything, our model predicts stronger deep circulation, and thus better ventilation, of the EMed in the past. Our model is driven by the present-day climate, i.e., corresponds to conditions close to a precession maximum. Sapropels are found to coincide with precession minima and are, as already stated, also observed for the Late Miocene. To the extent that sapropels indicate poor ventilation of deep water [*Cramp and O'Sullivan*, 1999; *Sancetta*, 1999; *Meyers and Negri*, 2003] the question arises how the Late Miocene deep circulation changes when we change the climate to precession minimum conditions. Does the presence of a strong deep cell at precession maximum make it less likely that the deep water turns stagnant at precession minimum? Perhaps it is rather that the greater surface area of the proto-Adriatic makes the basin in general more sensitive to the precession cycle and there is in fact a strong change in circulation when we move to precession minimum conditions. In general, we may suggest that investigation of the effect of precession-related climate variation for both the present day and the Late Miocene, given that sapropels are found in both situations, may yield valuable insight into the mechanism of sapropel formation.

[52] 3. While the fact that our control experiment proves unable to capture the deep circulation of the WMed tells us that our model is perhaps limited in this respect also for the Late Miocene, it is still interesting to observe in Figure 12 that the model for the Late Miocene no longer predicts a gyre in the northern WMed. Given that the present-day Lions gyre is thought to play an important role in driving the deep convection we may point out that the Late Miocene WMed perhaps lacked one of the conditions necessary for deep water formation.

[53] 4. Our results provide insight into the importance of several suggested paleogeographical alternatives. Specifically, the presence of shallow straits across the Corsica-Sardinia block and the absence of the Aegean Sea and the connection it provides to the Parathethys do not seem to affect the overall basin circulation. Their effects are limited to the immediate vicinity. In contrast, the sill depth between the western and eastern subbasins is found to strongly control the deep circulation of the EMed.

[54] 5. Our Late Miocene experiments with two gateways to the Atlantic, simple in planform and of equal and uniform depth, provide us with a convenient reference in thinking about the effects of gateway geometry. Both gateways are found to function like the present-day Strait of Gibraltar but, interestingly, we find the two straits do not handle an equal share of the total return flow to the Mediterranean. Fossil content and sedimentological aspects of deposits in and near the gateways have been interpreted to indicate different flow arrangements, for example, the presence of eastward flowing water at depth [e.g., *Benson et al.*, 1991; *Cunningham and Collins*, 2002; see also *Martín et al.*, 2001]. This would correspond to gateway geometries different from what we have considered in our modeling and may indeed relate to particular stages, just preceding the Messinian Crisis, for example.

[55] 6. The experiment including atmospheric forcing over the gateways to the Atlantic may have bearing on our understanding of the Messinian Salinity Crisis. These gateways are much different from the present-day strait of Gibraltar: they are long stretches of water and probably much more contorted than in our model representation [e.g., *Krijgsman*, 2002]. As shown by our model, on its way from the Atlantic to the Mediterranean the water already changes its properties; in particular, "Atlantic" water flowing into the WMed already has increased salinity. This may need to be taken into account in calculations of the salt budget of the Sea during the Messinian Crisis.

5. Conclusions

[56] To gain insight into the effect of paleogeography on the circulation of the Late Miocene Mediterranean Sea we have conducted numerical experiments of Mediterranean circulation using MOMA driven by present-day climatic forcing. Circulation computed for a Late Miocene paleogeography is compared to the circulation computed for the present, thereby allowing us to draw the following conclusions:

[57] 1. The model predicts Late Miocene circulation at surface/intermediate levels similar to what we have at present. There is eastward flow at the surface in all major straits and westward return flow at intermediate depth. Major changes in this upper thermohaline cell would have to be due to the factors not accounted for in our study: Atlantic gateway depth and/or climate different from present.

[58] 2. The Late Miocene configuration, in particular the greater area of the Adriatic Sea, is found to give rise to an increased deep circulation of the eastern subbasin.

[59] 3. Deepening of the Late Miocene connection between the western and eastern subbasin reduces deep circulation of the eastern basin.

[60] 4. The presence of shallow straits across the Miocene Corsica-Sardinia block and absence of the Aegean Sea and the access it provides to water of Parathethyan origin, appear to have only localized significance.

References

Beckers, J.-M., et al. (2002), Model intercomparison in the Mediterranean: MEDMEX simulations of the seasonal cycle, *J. Mar. Syst.*, *33–34*, 215–251.

Benson, R. H., K. RaKic-El Bied, and G. Bonaduce (1991), An important current reversal (influx) in the Rifian corridor (Morocco) at the Tortonian-Messinian boundary: The end of the Tethys ocean, *Paleoceanography*, *6*, 164–192.

Bethoux, J.-P. (1984), Paleoceanographic changes in the Mediterranean Sea in the last 20,000 years, *Oceanol. Acta*, *7*, 43–48.

Bethoux, J. P., and B. Gentili (1999), Functioning of the Mediterranean Sea: Past and present changes related to freshwater input and climate changes, *J. Mar. Syst.*, *20*, 33–47.

Bethoux, J. P., B. Gentili, P. Morin, E. Nicolas, C. Pierre, and D. Ruiz-Pino (1999), The Mediterranean Sea: A miniature ocean for climatic and environmental studies and a key for the climatic functioning of the North Atlantic, *Progr. Oceanogr.*, *44*, 131–146.

Bice, K. L., C. R. Scotese, D. Seidov, and E. J. Barron (2000), Quantifying the role of geographic change in Cenozoic ocean heat transport using uncoupled atmosphere and ocean models, *Palaeogeogr. Palaeoclimatol. Palaeoecol.*, *161*, 295–310.

Bigg, G. R. (1994), An ocean general circulation model view of the glacial Mediterranean thermohaline circulation, *Paleoceanography*, *9*, 705–722.

Bignami, F., S. Marullo, R. Santoleri, and M. E. Schiano (1995), Longwave radiation budget in the Mediterranean Sea, *J. Geophys. Res.*, *100*, 2501–2514.

Bjerrum, C. J., F. Surlyk, J. H. Callomon, and R. L. Slingerland (2001), Numerical paleoceanographic study of the Early Jurassic transcontinental Laurasian seaway, *Paleoceanography*, *16*, 390–404.

Brasseur, P., J. M. Beckers, J. M. Brankart, and R. Schoenauen (1996), Seasonal temperature and salinity fields in the Mediterranean Sea: Climatological analyses of an historical data set, *Deep Sea Res. Part I*, *43*, 159–192.

Bryden, H. L., and T. H. Kinder (1991), Steady two-layer exchange through the Strait of Gibraltar, *Deep Sea Res.*, *38*, S445–S463.

Budyko, M. I. (1963), *Atlas of the Heat Balance of the Earth* (in Russian), Glabnaia Geofiz. Observ., A. I. Voeikova, Moscow.

Castellari, S., N. Pinardi, and K. Leaman (1998), A model study of air-sea interactions in the Mediterranean Sea, *J. Mar. Syst.*, *18*, 89–114.

Castellari, S., N. Pinardi, and K. Leaman (2000), Simulation of water mass formation processes in the Mediterranean Sea: Influence of the time frequency of the atmospheric forcing, *J. Geophys. Res.*, *105*, 24,157–24,181.

Cramp, A., and G. O'Sullivan (1999), Neogene sapropels in the Mediterranean: A review, *Mar. Geol.*, *153*, 11–28.

Cunningham, K. J., and L. S. Collins (2002), Controls on facies and sequence stratigraphy of an upper Miocene carbonate ramp and platform, Melilla basin, NE Morocco, *Sediment. Geol.*, *146*, 285–304.

Dercourt, J., M. Gaetani, B. Vrielynck, E. Barrier, B. Biju-Duval, M. F. Brunet, J. P. Cadet, S. Crasquin, and M. Sandulescu (Eds.) (2000), *Peri-Tethys Atlas: Palaeogeographical Maps*, Comm. for the Geol. Map of the World, Paris.

Duggen, S., K. Hoernle, P. van den Bogaard, L. Rüpke, and J. Phipps Morgan (2003), Deep roots of the Messinian salinity crisis, *Nature*, *422*, 602–606.

Haines, K., and P. Wu (1995), A modelling study of the thermohaline circulation of the Mediterranean Sea: Water formation and dispersal, *Oceanol. Acta*, *18*, 401–417.

Haines, K., and P. Wu (1998), GCM studies of intermediate and deep-waters in the Mediterranean, *J. Mar. Syst.*, *18*, 197–214.

Hellerman, S., and M. Rosenstein (1983), Normal wind stress over the world ocean with error estimates, *J. Phys. Oceanogr.*, *13*, 1093–1104.

Hilgen, F. J. (1991), Astronomical calibration of Gauss to Matuyama sapropels in the Mediterranean and implication for the geomagnetic polarity time scale, *Earth Planet. Sci. Lett.*, *104*, 226–244.

Jaeger, L. (1976), Monatskarten des Niederschlags für die ganze Erde, *Ber. Dtsch. Wetterdienste*, *139*.

Johnson, R. G. (1997), Climate control requires a dam at the strait of Gibraltar, *Eos Trans. AGU*, *78*, 277–284.

Korres, G., and A. Lascaratos (2003), A one-way nested, eddy-resolving model of the Aegean and Levantine basins: Implementation and climatological runs, *Annal. Geophys.*, *21*, 205–220.

Korres, G., N. Pinardi, and A. Lascaratos (2000), The ocean response to low-frequency interannual atmospheric variability in the Mediterranean Sea, part I: Sensitivity experiments and energy analysis, *J. Clim.*, *13*, 705–731.

Kouwenhoven, T. J., and G. J. van der Zwaan (2004), A reconstruction of late Miocene Mediterranean circulation patterns using benthic foraminifera, *Palaeogeogr. Palaeoclimatol. Palaeoecol*, in press.

Kouwenhoven, T. J., M.-S. Seidenkrantz, and G. J. van der Zwaan (1999), Deep-water changes: The near-synchronous disappearance of a group of benthic foraminifera from the late Miocene Mediterranean, *Palaeogeogr. Palaeoclimatol. Palaeoecol.*, *152*, 259–281.

Kouwenhoven, T. J., F. J. Hilgen, and G. J. van der Zwaan (2003), Late Tortonian-early Messinian stepwise disruption of the Mediterranean-Atlantic connections: Constraints from benthic foraminiferal and geochemical data, *Palaeogeogr. Palaeoclimatol. Palaeoecol.*, *198*, 303–319.

Krijgsman, W. (2002), The Mediterranean: Mare nostrum of earth sciences, *Earth Planet. Sci. Lett.*, *205*, 1–12.

Krijgsman, W., F. J. Hilgen, I. Raffi, F. J. Sierro, and D. S. Wilson (1999), Chronology, causes and progression of the Messinian salinity crisis, *Nature*, *400*, 652–655.

Martín, J. M., J. C. Braga, and C. Betzler (2001), The Messinian Guadalhorce corridor: The last northern, Atlantic-Mediterranean gateway, *Terra Nova*, *13*, 418–424.

Meyers, P. A., and A. Negri (2003), Introduction to ''Paleoclimatic and Paleoceanographic Records in Mediterranean Sapropels and Mesozoic Black Shales,''*Palaeogeogr. Palaeoclimatol. Palaeoecol.*, *190*, 1–8.

Myers, P. G. (2002), Flux-forced simulations of the paleocirculation of the Mediterranean, *Paleoceanography*, *17*(1), 1009, doi:10.1029/2000PA000613.

Myers, P. G., and K. Haines (2000), Seasonal and interannual variability in a model of the Mediterranean under derived flux forcing, *J. Phys. Oceanogr.*, *30*, 1069–1082.

Myers, P. G., K. Haines, and E. J. Rohling (1998), Modeling the paleocirculation of the Mediterranean: The last glacial maximum and the Holocene with emphasis on the formation of sapropel S_1, *Paleoceanography*, *13*, 586–606.

Pacanowski, R. C., and S. M. Griffies (1998), *MOM 3.0 Manual*, NOAA/Geophys. Fluid Dyn. Lab., Princeton, N. J.

Pinardi, N., and E. Masetti (2000), Variability of the large scale general circulation of the Mediterranean Sea from observations and modelling: A review, *Palaeogeogr. Palaeoclimatol. Palaeoecol.*, *158*, 153–174.

Poulsen, C. J., E. J. Barron, M. A. Arthur, and W. H. Peterson (2001), Response of the mid-Cretaceous global oceanic circulation to tectonic and CO_2 forcings, *Paleoceanography*, *16*, 576–592.

Reed, R. K. (1977), On estimating insolation over the ocean, *J. Phys. Oceanogr.*, *17*, 854–871.

Rögl, F. (1999), Circum-Mediterranean Miocene paleogeography, in *The Miocene Land Mammals of Europe*, edited by G. E. Rossner and K. Heissig, pp. 39–48, Pfeil, Munich.

Rossignol-Strick, M. (1983), African monsoons, an immediate climate response to orbital insolation, *Nature*, *304*, 46–49.

Roussenov, V., E. Stanev, V. Artale, and N. Pinardi (1995), A seasonal model of the Mediterranean Sea general circulation, *J. Geophys. Res.*, *100*, 13,515–13,538.

Sancetta, C. (1999), The mystery of the sapropels, *Nature*, *398*, 27–29.

Seidenkrantz, M.-S., T. J. Kouwenhoven, F. J. Jorissen, N. J. Shackleton, and G. J. van der Zwaan (2000), Benthic foraminifera as indicators of changing Mediterranean-Atlantic water exchange in the late Miocene, *Mar. Geol.*, *163*, 387–407.

Sierro, F. J., J. A. Flores, G. Francés, A. Vazquez, R. Utrilla, I. Zamarreño, H. Erlenkeuser, and M. A. Barcena (2003), Orbitally controlled oscillations in planktic communities and cyclic changes in western Mediterranean hydrography during the Messinian, *Palaeogeogr. Palaeoclimatol. Palaeoecol.*, *190*, 289–316.

Slingerland, R., L. R. Kump, M. A. Arthur, P. J. Fawcett, B. B. Sageman, and E. J. Barron (1996), Estuarine circulation in the Turonian Western Interior seaway of North

America, *Geol. Soc. Am. Bull.*, *108*, 941–952.

Smith, W. H. F., and P. Wessel (1990), Gridding with continuous curvature splines in tension, *Geophysics*, *55*, 293–305.

Stratford, K., R. G. Williams, and P. G. Myers (2000), Impact of the circulation on sapropel formation in the eastern Mediterranean, *Global Biochem. Cycles*, *14*, 683–695.

van der Meulen, M. J., T. J. Kouwenhoven, G. J. van der Zwaan, J. E. Meulenkamp, and M. J. R. Wortel (1999), Late Miocene uplift in the

Romagnan Apennines and the detachment of subducted lithosphere, *Tectonophysics*, *315*, 319–335.

Webb, D. J. (1996), An ocean model code for array processor computers, *Compu. Geosci.*, *22*, 569–578.

Wessel, P., and W. H. F. Smith (1998), New, improved version of Generic Mapping Tools released, *EOS Trans. AGU*, *79*, 579.

Wu, P., and K. Haines (1998), The general circulation of the Mediterranean Sea from a 100-year simulation, *J. Geophys. Res.*, *103*, 1121–1135.

Zavatarelli, M., and G. L. Mellor (1995), A numerical study of the Mediterranean circulation, *J. Phys. Oceanogr.*, *25*, 1384–1414.

————————————

P. Th. Meijer and M. J. R. Wortel, Vening Meinesz Research School of Geodynamics, Faculty of Geosciences, Utrecht University, PO Box 80 021, 3508 TA Utrecht, Netherlands. (meijer@geo.uu.nl)

R. Slingerland, Department of Geosciences, Pennsylvania State University, University Park, PA 16802-2714, USA. (sling@geosc.psu.edu)
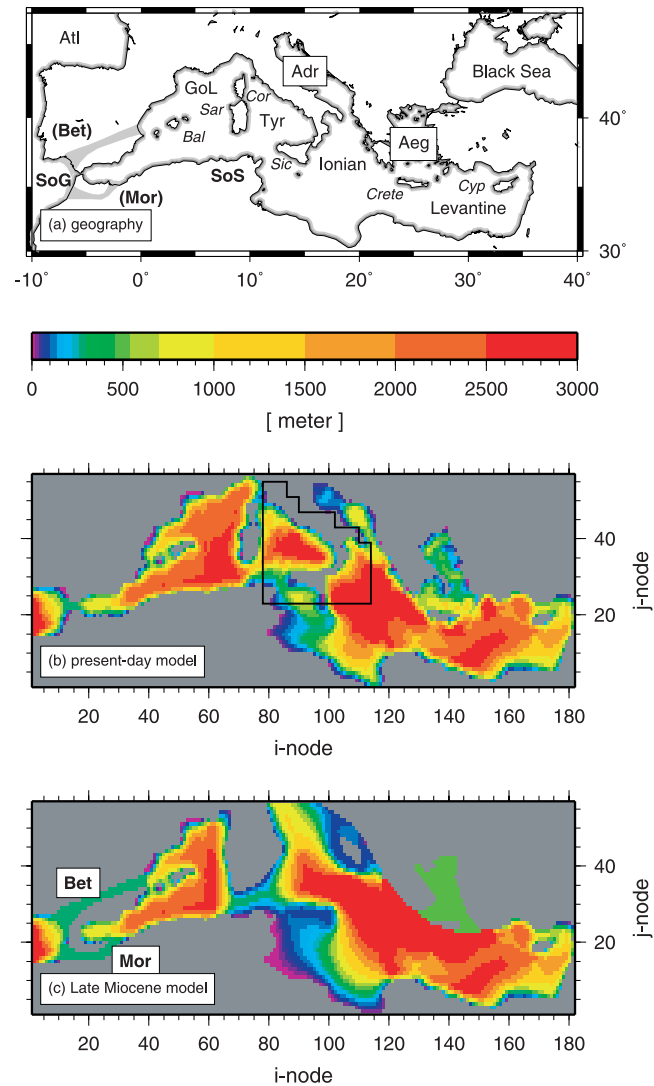
Figure 1. (top) Geographical names used in the text. The approximate position of the Late Miocene Atlantic gateways is also shown (shaded). Key: Adr, Adriatic Sea; Aeg, Aegean Sea; Atl, Atlantic Ocean; Bal, Balearic islands; Bet, Betic gateway, Cor, Corsica; Cyp, Cyprus; GoL, Gulf of Lions; Mor, Moroccan gateway; Sar, Sardinia; Sic, Sicily; SoG, Strait of Gibraltar; SoS, Strait of Sicily; Tyr, Tyrrhenian Sea. (middle) Model bathymetry for the present day. The black contour delimits the area for which atmospheric data are masked. (bottom) Model bathymetry for the Late Miocene (reference paleogeography). Key: Bet, Betic gateway, Mor, Moroccan gateway.
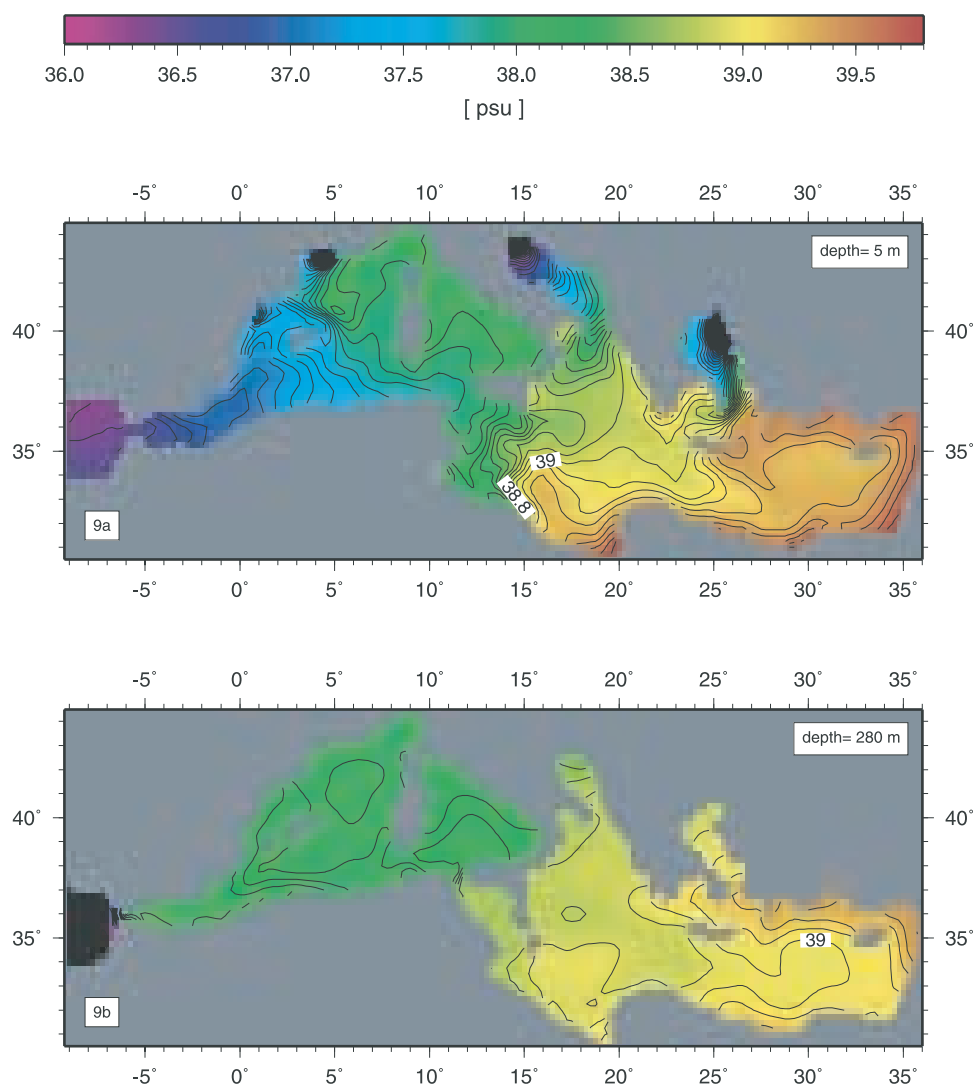
Figure 9. Horizontal slices through the modeled salinity field at the surface (5 m) and at 280 m; mean of year 15 of the control experiment. Land area is gray; black indicates salinity below 36 psu (due to rivers). Contour interval is 0.1 psu.
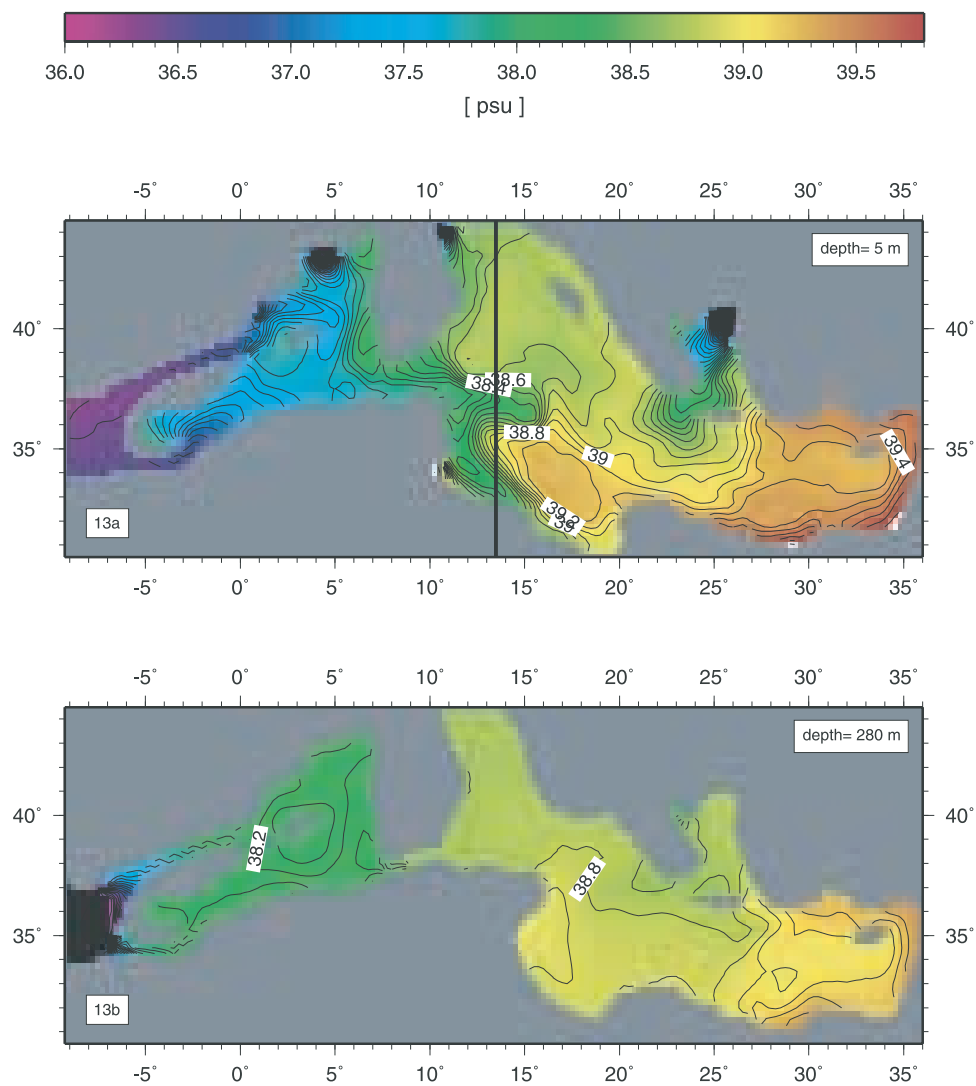
Figure 13. Horizontal salinity fields at the surface and 280 m; Late Miocene experiment (reference paleorun). Annual mean of year 15. Contour interval is 0.1 psu. Bold line indicates section of Figure 14.
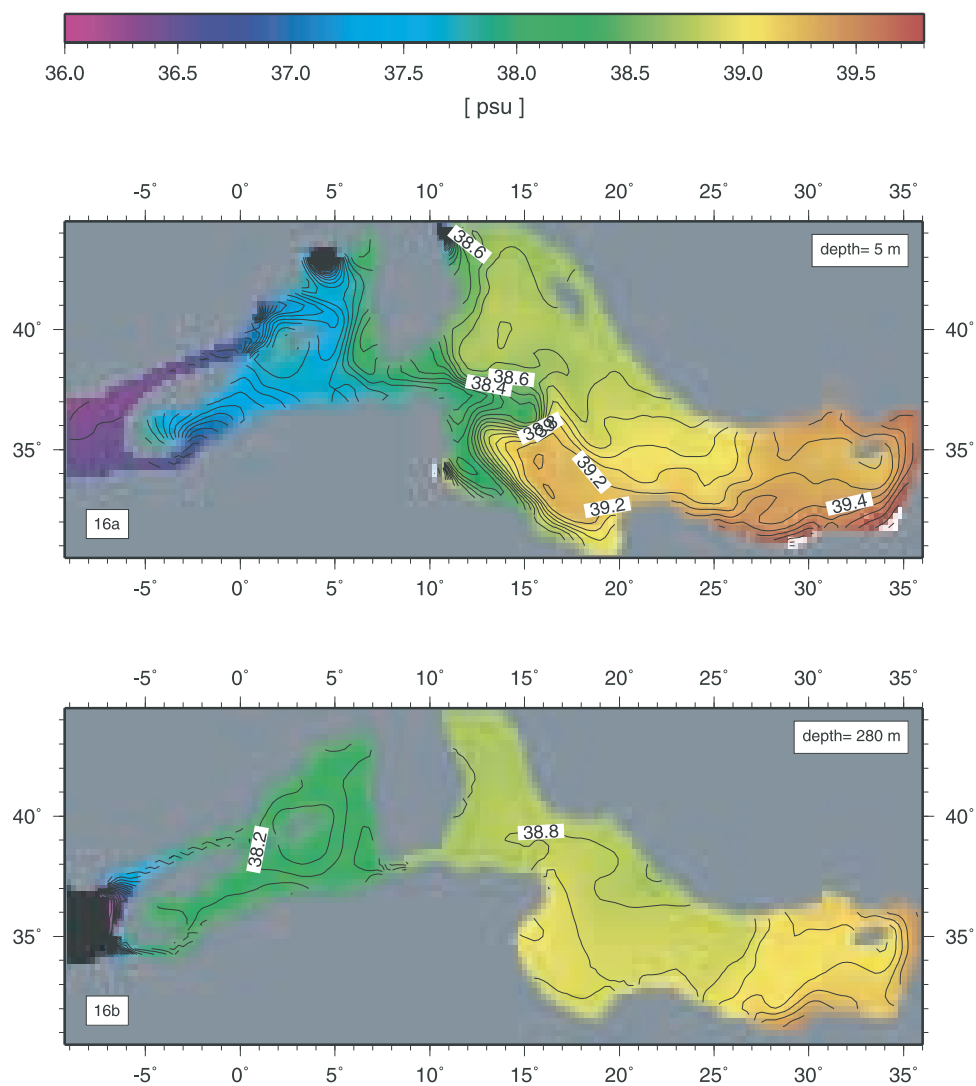
Figure 16. Horizontal salinity fields at the surface and 280 m; Late Miocene experiment without Aegean Sea. Annual mean year 15. Contour interval is 0.1 psu.